NAVAL POSTGRADUATE SCHOOL

MONTEREY, CALIFORNIA

THESIS

MICROSTRUCTURAL SURFACE INCORPORATION OF PHASE CHANGE MATERIALS FOR THERMAL MANAGEMENT APPLICATIONS

by

Christopher J. Anderson

June 2022

Thesis Advisor: Claudia C. Luhrs
Second Reader: Troy Ansell

THIS PAGE INTENTIONALLY LEFT BLANK

REPORT DOCUMENTATION PAGE			*Form Approved OMB No. 0704-0188*

1. AGENCY USE ONLY *(Leave blank)*	**2. REPORT DATE** June 2022	**3. REPORT TYPE AND DATES COVERED** Master's thesis

4. TITLE AND SUBTITLE MICROSTRUCTURAL SURFACE INCORPORATION OF PHASE CHANGE MATERIALS FOR THERMAL MANAGEMENT APPLICATIONS	**5. FUNDING NUMBERS** RMQ80; RML1H
6. AUTHOR(S) Christopher J. Anderson	
7. PERFORMING ORGANIZATION NAME(S) AND ADDRESS(ES) Naval Postgraduate School Monterey, CA 93943-5000	**8. PERFORMING ORGANIZATION REPORT NUMBER**
9. SPONSORING / MONITORING AGENCY NAME(S) AND ADDRESS(ES) ESTEP, Monterey, CA 93943	**10. SPONSORING / MONITORING AGENCY REPORT NUMBER**

11. SUPPLEMENTARY NOTES The views expressed in this thesis are those of the author and do not reflect the official policy or position of the Department of Defense or the U.S. Government.

12a. DISTRIBUTION / AVAILABILITY STATEMENT Approved for public release. Distribution is unlimited.	**12b. DISTRIBUTION CODE** A

13. ABSTRACT (maximum 200 words)

Thermal management strategies employed to mitigate the detrimental effects of elevated temperatures include the use of heat sinks or spreaders, thermal interface materials, and phase change materials (PCM), among others. PCM are substances capable of absorbing or releasing thermal energy when they undergo a phase transition. The goal of this thesis was to engineer a surface layer that contained a phase change material on top of a metallic component used for thermal dissipation and test its performance. The ideal conditions to create a porous anodic layer that could contain phase change material in an aluminum substrate were determined. Vacuum impregnation was used to incorporate the phase change material within the annealed anodic layer. Sealing materials were tested regarding their effectiveness to contain the PCM, their thermal conductivity and ability to withstand thermal cycles. Thermal tests were run to compare the behavior of samples containing PCM with those that were only anodized and raw aluminum. The use of the alkane eicosane as PCM, introduced in pores created by anodization techniques in an aluminum heat sink that served as substrate, resulted in specimens that presented lower temperatures during the heating cycles than those without PCM, proving the potential of this strategy to manage transient thermal loads.

14. SUBJECT TERMS phase change material, PCM, latent energy storage, heat sink, aluminum heat sink, CPU cooling, eicosane, anodization techniques, passive thermal management	**15. NUMBER OF PAGES** 87
	16. PRICE CODE

17. SECURITY CLASSIFICATION OF REPORT	**18. SECURITY CLASSIFICATION OF THIS PAGE**	**19. SECURITY CLASSIFICATION OF ABSTRACT**	**20. LIMITATION OF ABSTRACT**
Unclassified	Unclassified	Unclassified	UU

NSN 7540-01-280-5500

Standard Form 298 (Rev. 2-89)
Prescribed by ANSI Std. 239-18

THIS PAGE INTENTIONALLY LEFT BLANK

Approved for public release. Distribution is unlimited.

MICROSTRUCTURAL SURFACE INCORPORATION OF PHASE CHANGE MATERIALS FOR THERMAL MANAGEMENT APPLICATIONS

Christopher J. Anderson
Lieutenant, United States Navy
BS, United States Naval Academy, 2012

Submitted in partial fulfillment of the
requirements for the degree of

MASTER OF SCIENCE IN MECHANICAL ENGINEERING

from the

NAVAL POSTGRADUATE SCHOOL
June 2022

Approved by: Claudia C. Luhrs
Advisor

Troy Ansell
Second Reader

Garth V. Hobson
Chair, Department of Mechanical and Aerospace Engineering

THIS PAGE INTENTIONALLY LEFT BLANK

ABSTRACT

Thermal management strategies employed to mitigate the detrimental effects of elevated temperatures include the use of heat sinks or spreaders, thermal interface materials, and phase change materials (PCM), among others. PCM are substances capable of absorbing or releasing thermal energy when they undergo a phase transition. The goal of this thesis was to engineer a surface layer that contained a phase change material on top of a metallic component used for thermal dissipation and test its performance. The ideal conditions to create a porous anodic layer that could contain phase change material in an aluminum substrate were determined. Vacuum impregnation was used to incorporate the phase change material within the annealed anodic layer. Sealing materials were tested regarding their effectiveness to contain the PCM, their thermal conductivity and ability to withstand thermal cycles. Thermal tests were run to compare the behavior of samples containing PCM with those that were only anodized and raw aluminum. The use of the alkane eicosane as PCM, introduced in pores created by anodization techniques in an aluminum heat sink that served as substrate, resulted in specimens that presented lower temperatures during the heating cycles than those without PCM, proving the potential of this strategy to manage transient thermal loads.

THIS PAGE INTENTIONALLY LEFT BLANK

TABLE OF CONTENTS

LIST OF FIGURES

THIS PAGE INTENTIONALLY LEFT BLANK

LIST OF TABLES

THIS PAGE INTENTIONALLY LEFT BLANK

LIST OF ACRONYMS AND ABBREVIATIONS

AAO	Aluminum Anodic Oxide
CPU	Central Processing Unit
DARPA	Defense Advanced Research Projects Agency
DI	De Ionized
DOD	Department of Defense
EDS	Energy Dispersive X-ray Spectroscopy
FLIR	Forward Looking Infra-Red
HR	Heat Resistant
HVAC	Heating Ventilating Air Conditioning
LEO	Low Earth Orbit
LTES	Latent Thermal Energy Storage
MEPCM	Micro Encapsulated Phase Change Material
NASA	National Air and Space Administration
PCM	Phase Change Material
RPM	Rotations Per Minute
RTV	Room Temperature Vulcanizing
SEM	Scanning Electron Microscopy
Tm	Effective Melting Temperature

THIS PAGE INTENTIONALLY LEFT BLANK

EXECUTIVE SUMMARY

Multiple Department of Defense (DOD) platforms require high power or high speeds as well as situations that expose their components to elevated temperatures, which could compromise their functionality. Thermal runaway in batteries, central processing unit (CPU) overheat, and ablation of materials are common examples of the negative effects that high temperatures could promote. Thermal management strategies employed to mitigate the detrimental effects of elevated temperatures include the use of heat sinks or spreaders, thermal interface materials, and phase change materials (PCM), among others. PCM are substances capable of absorbing or releasing thermal energy when they undergo a phase transition.

The goal of this thesis was to engineer a surface layer that contained a phase change material on top of a metallic component used for thermal dissipation and test its performance. The ideal conditions to create a porous anodic layer that could contain phase change material in a metallic substrate were determined. Vacuum impregnation was used to incorporate the phase change material within the annealed anodic layer. Sealing materials were tested regarding their effectiveness to contain the PCM, their thermal conductivity and ability to withstand thermal cycles. Thermal tests were run to compare the behavior of samples containing PCM with those that were only anodized and raw aluminum. The use of the alkane eicosane as PCM, introduced in pores created by anodization techniques in an aluminum heat sink that served as substrate, resulted in specimens that presented lower temperatures during the heating cycles than those without PCM, proving the potential of this strategy to manage transient thermal loads.

THIS PAGE INTENTIONALLY LEFT BLANK

ACKNOWLEDGMENTS

I would like to give thanks to my thesis advisor, Dr. Claudia Luhrs, who inspired this work. Her guidance in the lab, throughout characterization and testing, and with writing has been invaluable. Additionally, the courses I took from her were incredibly helpful for this entire thesis. At the end of every course, I did not just know about the processes involved with material science manufacturing and fabrication, but I knew how to do them. I would also like to thank my second reader, Dr. Troy Ansell, who trained me to use multiple pieces of equipment for analysis that were critical for this thesis. He was always available for advice when needed in the lab and assisted with operation of equipment and analysis of specimens to help overcome unexpected obstacles. I would also like to thank Forest Shaner, who assisted with multiple tasks during his internship. Thank you to every professor I had that gave me the tools to tackle this thesis. Without the knowledge gained from your courses, I would not have known how to design multiple testing apparatus, overcome obstacles, or understand the results from these conducted tests.

I would also like to give special thanks to my wife who spent many nights at home alone while I worked in the lab or was in my office writing. If it wasn't for the drive and inspiration she gave me, I would not have made it to Naval Postgraduate School in the first place. Lastly, I would like to thank a fellow Naval Officer, LCDR Keith Loedeman, who is also enrolled at Naval Postgraduate School. Keith taught me how to fabricate fiberglass surfboards in his garage. This fabrication process involved gradient polishing, chemical and mechanical epoxy bonding, and vacuum impregnation of epoxies in fiberglass which were all related skills to the preparation and sealing of these phase change induced anodic layers.

THIS PAGE INTENTIONALLY LEFT BLANK

I. INTRODUCTION

A. OVERVIEW

Thermal management has a major impact in today's world. Buildings are thermally managed to condition the air and make it more comfortable for those working and living in them. Machines are managed via oil and heat exchanging systems that prevent them from overheating which would cause structural failure. Electrical components are cooled via forced or free convection to prevent capacitors and transistors from melting, rendering them incapable of computing.

In this thesis, organic phase change materials were integrated in the surface layer of a metallic component and used to absorb thermal energy. Their integration was accomplished via a simple post manufacturing process that can be applied to existing parts such as heat sinks that assist in thermal management, for not only machines such as differentials and engines, but also nano applications in Central Processing Units (CPU's) and electronic devices that experience cyclic thermal loads.

This chapter provides a brief introduction to thermal management systems, the basic definition of phase change materials (PCMs), and how they will be applied to this field of research in a novel way. Examples of how PCMs can provide superior thermal management to parts that previously depended upon thermal dissipation alone to protect surrounding parts and equipment are presented. Lastly, a brief introduction of sealant methods and their importance to the current work will be discussed.

B. THERMAL LOAD MANAGEMENT APPLICATION AND BACKGROUND

1. Thermal Management Systems

There are many types of thermal management systems to include active and passive systems as well as macro and nano systems. An active type of thermal management system would be one that uses or depends on equipment to move a fluid to exchange heat and cool down a space or piece of equipment. Examples of active systems are refrigeration systems that pump R-114 through a pump to absorb heat from one side of the system and give heat

off on the other side of the system. These systems are designed for DDG-51 class ships [1]. Other active systems may include a fan that forces air over a piece of equipment using forced convection to cool the system down as it heats up. Applications of active cooling techniques require additional design and power requirements which results in high operating costs [2]. Industries have been applying passive cooling systems to cut costs on energy usage while reducing the impact on the design of equipment. These passive energy systems are either materials or geometries applied to equipment such as finned heat sinks with large surface areas that can improve the rate of heat dissipation a component can experience during operation. A passive energy system that is promising to many fields is the use of PCMs. Examples of such can be found in applications that relate to electronics, fabrics, cold storage, medical, and many others that are of interest to DOD fields of work which are mentioned in sections ahead [3]–[8].

a. Phase Change Material Definition

PCMs store and release heat at temperatures at or near their phase change temperatures. These phase changes are endothermic while heating from solid to liquid, and exothermic upon cooling from liquid back to solid. During the phase change process from solid to liquid, a constant temperature is maintained. This constant temperature allows for application in latent thermal energy storage (LTES) and thermal management systems. PCM's have been applied in heat recovery, solar [9], aerospace, buildings [10], textiles [8], and electronics [11].

Solid-liquid PCM's are used due to their low density and small change in volume during phase changes. PCM's can be divided into three categories, organic, inorganic, and eutectics. Organic PCM's include alcohol, sugar, paraffin, and fatty acids to list a few examples. Water, salt, and metals are some examples of inorganic PCM's. Two or more miscible components combined are called eutectics [11].

Paraffin waxes are composed of a straight chain of n-alkanes $CH_3–(CH_2)_n–CH_3$. The crystallization of the hydrocarbon chain releases a large amount of latent heat. The melting point and latent heat of fusion increase with chain length, which allows for paraffin waxes to be available in a large temperature range [12]. Furthermore, paraffins are safe,

predictable, relatively cheap, non-corrosive, and self-nucleating. Self-nucleation means they will crystallize with little or no supercooling (i.e., cooling below a phase transition temperature, typically the solidification temperature). They do have low thermal conductivity [12] and any application of them will need to be accounted for in the design of the LTES device.

b. Active vs Passive Thermal Management Systems

Most buildings use active cooling to regulate their temperatures. These active systems require large amounts of energy. The European Union has seen an increase in energy demand that is equivalent to 1084 million tons of oil. Buildings account for 33.33% of the energy consumption globally and are considered a major source of CO_2 emissions. This is due to their active heating, ventilating, and air conditioning (HVAC) systems that require large amounts of power to operate [13]. With the advantages that phase change materials present to the application of passive energy systems, buildings' cooling systems could see a major reduction in energy costs by applying this technology to building materials.

Examples of PCM applicability include a study done by the International University of Beirut looked into the application of phase change materials and concluded that by incorporating layers of enclosed phase change materials could serve as thermal buffers that can reduce the thermal peaks experienced by HVAC systems during peak hot and cold temperatures [13]. Silva et al. [14] performed an experimental study on the performance of aluminum window blinds that were incorporated with phase change materials. Their results indicated that the PCM induced shutters decreased the maximum indoor temperature of 8.7% and an increase of 16.7% in the minimum indoor temperature at night. With the combination of active cooling systems, as well as PCM induced materials, this greatly reduced the energy load of the HVAC system. This is all because of latent heat energy storage. This latent heat causes the temperature rate to significantly decrease during the PCM's effective melting temperature T_m. This decrease in the rate of heating is shown in Figure 1, which is provided by Faraj et al. [13].

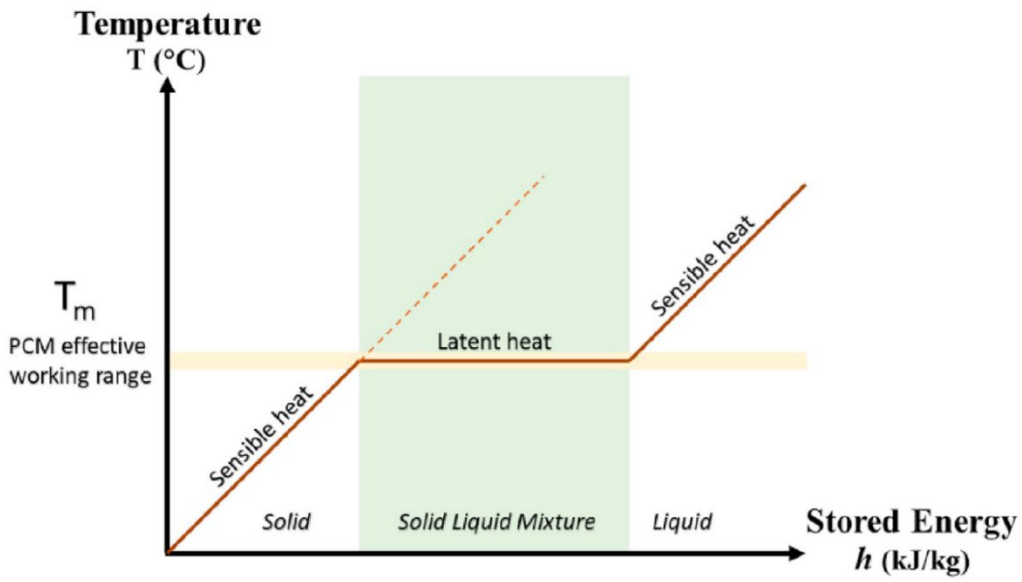

Figure 1. Heat storage as latent heat prevents temperature increase throughout the phase changing state of the PCM. Source: [13].

Other studies went on to calculate the energy demands and savings related to the use of PCMs incorporated in the walls of deployable dwellings made from shipping containers. By developing and using epoxy-PCM filler composites, a total energy saving of 16 to 23 percent was attained. This concept is especially valuable in situations that would need deployable buildings, such as those encountered after natural disasters or for armed forces operations in locations where the supply of energy is limited [15].

This wall design has been applied to many studies that sandwich PCM, incorporated amongst a composite material, between the inside and outside of a building. In another study, conducted by Isa et al. [16], used a copper foam that would be sandwiched between bricks to the outside and hygrothermal wallboard that would increase thermal conductivity to the inside. Lastly, ventilation holes were incorporated into the top of the wall to exhaust heat upon solidification of the phase change material at night. The design is shown in Figure 2.

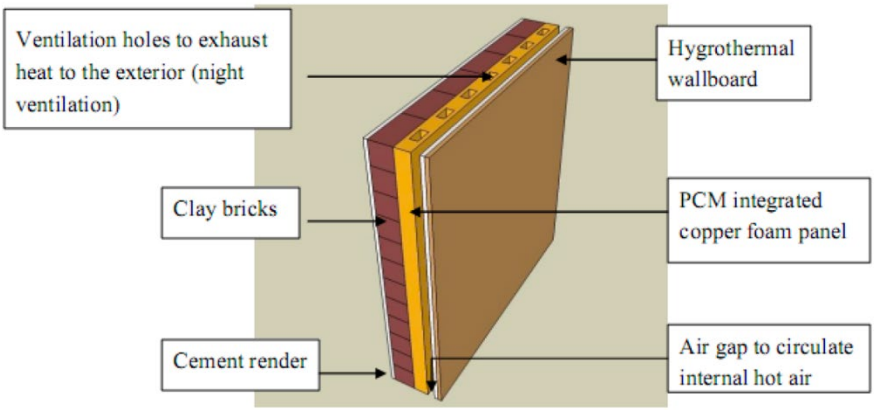

Figure 2. Wall materials with copper foam integrated PCM. Source: [16].

This is a large volume application of passive heat management systems but shows promise and reflects the overall concept of the use of these passive systems very well.

c. Applications of PCM to Electrical Systems

Due to the limited space and power available in computers or electronic devices, passive systems such as heat dissipating fins incorporated in existing designs are used to dissipate heat more effectively without requiring more energy or space from a system. Heat pipes like the ones shown in Figure 3 are passive heat transfer devices with an extremely high effective thermal conductivity [17].

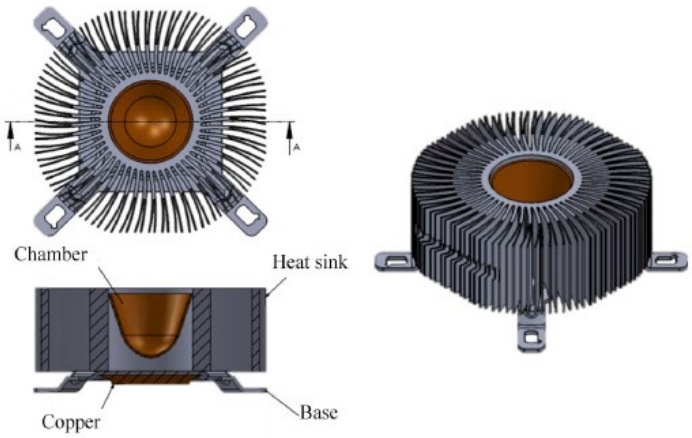

Figure 3. Schematic diagram of heat pipe embedded with heat sink unit. Source: [17].

The complex geometry of the heat sink is used to increase the surface area, which greatly increases the rate of heat dissipation that the surrounding equipment experiences [18]. These heat sinks are not just used on CPUs, but on large pumps, auxiliary machine equipment, and various engines [19], to name a few examples of many where these complex fins are applied. With the use of PCM's, these heat sinks could absorb the thermal energy of the equipment around them as LTES devices.

(1) Orion Space Craft

Another application of this concept was applied to NASA's (National Air and Space Administration) Orion Multi-Purpose Crew Vehicle to create a thermally self-sufficient system by using PCM to store waste heat. The maximum recommended operating temperature for the electronics on the spacecraft is 30 ºC to 40 ºC. Octadecane was chosen as a PCM that changes phase just below the maximum operating temperature of this equipment, 28 ºC. This temperature range was chosen since the cabin air is maintained at 26.7 ºC for human comfort [20]. During the use of the science communication suite, the waste heat from the payload will melt the paraffin wax at a constant temperature, resembling the latent heat phase from Figure 1. Octadecane, which is integrated in a macro honeycomb structure of aluminum panels of 35.6 cm x 35.6 cm x 1 cm can absorb 100 W of waste heat given off by the electronics and the PCM had no degradation after 5,000 thermal cycles. NASA estimated that the effect lasted for one hour before the equipment was required to be turned off to allow the PCM to solidify again. This system was designed to remove the dependance on the cold plate heat sink of the Orion Crew Module, which are a single point of failure without the PCM panels [20]. This system was further developed to an active/passive PCM heat exchanger which can hold up to 10 lbs. of PCM placed around a tube which pumps a mixture of propylene glycol and water from the equipment between temperatures of -10 ºC and 30 ºC. When the coolant is hot, it causes a the PCM to change phase and cools the mixture before going back to the electronics heat exchanger. The heat exchanger is about one fifth the size of the previously designed active system used on Orion. When the orbit transitions to the dark side of the moon, Orion's radiators will refreeze the PCM for its repeated use on the moon's hot side [21]. The PCM heat exchanger module is shown in Figure 4.

Figure 4. Removable drawer that can store up to 4.5 kg of PCM in aluminum panels. Source: [21].

While these examples show that phase change materials can be used to save energy in passive systems or reduce the size of equipment in active systems, they both require significant design considerations when applying this technology to accomplish its goals. These designs can be minimized for smaller scale application. Smaller configurations could be applied to many technologies ranging from those with DOD interest, to personal use electronics. The use of PCMs increases the effectiveness of passive thermal management systems without significantly increasing its original design footprint or functionality.

(2) Enhancement of coolant with PCMs

Another study of paraffin application intended to combine with active/ passive heat transfer systems was micro-encapsulated PCM's (MEPCM's) in water. N-Eicosane PCM's coated with urea-formaldehyde polymer shells were suspended in water to increase the latent heat values [22]. This MEPCM water mixture was used in an existing heat exchanger. The encapsulated PCM was proven to absorb more thermal energy from the surrounding equipment than just water, therefore, contributing to a more effective and more efficient thermal management system. When the temperature of the MEPCM phase change region was below or above the phase change, there was an overall decrease in the latent heat energy values [22], which indicate the equipment operating temperature is an

extremely important design consideration for the selection of PCMs. This system, while effective in a specific temperature region, requires the existence of an active thermal management system, which still uses excess power and space than a passive system.

d. Overall Case for PCMs

PCM usage across diverse studies found in the literature demonstrated that PCM can decrease peak loads in cyclic thermal management cycles. In addition, they could be selected so their T_m is just below peak operating temperature, like the case with the PCMs used on the Orion Spacecraft science communication suite. PCMs employed as passive thermal management systems have great potential to protect surrounding equipment from peak loads that would cause catastrophic failure, increasing the efficiency of existing thermal management systems, and decreasing the size of complex parts that would otherwise alter the design of an existing system in a detrimental way.

e. Case for Use of PCMs in DOD Applications

Examples of DOD applicability of PCM within the past decade include the Defense Advanced Research Projects Agency (DARPA) pursuit of micro and nanotechnology to reduce thermal management constraints of DOD electronic systems. The DARPA thermal management program conducts multiple fields of research to include micro technologies for air cooled exchangers, nano-thermal interfaces, active cooling modules, and thermal transport systems. High performance heat spreaders that use phase change processes to replace copper-alloy heat distributors can be applied to every category of use within the thermal management technology program. Thermal management performance of existing designs which serve the DOD and military systems can be constrained thermally by either high usage scenarios or because of geographical areas where operations occur. Improving these thermal management technologies would improve their maximum thermal load capacities and dependability whether at home or overseas [23].

2. Thesis Objective and Hypothesis

The goal of this study was to engineer a metallic microstructural surface layer that incorporated PCM through a simple postproduction process that could be applied to

existing, geometrically complex parts. To accomplish this, a fabrication route able to generate porous structures without damaging the host structure or reducing its mechanical robustness had to be identified. These micro channels would need to be able to accept the phase change material and be strong enough to sustain the various forces placed upon them in the fabrication process. Lastly, this material would need to sustain multiple thermal cycles. Therefore, a method of sealing the PCM within the anodic layer should employed to prevent leakage of the PCM upon heating but use materials thermally conductive to decrease the temperature of its surroundings.

The utility of microstructural PCM induction is to increase the efficacy of existing passive thermal management systems, reduce the use of active thermal management systems, and be applied to sizes of equipment from nano scaled computer chips to larger equipment without affecting the functionality or design. This thesis is a proof of concept of the effectiveness of incorporating PCM within the surface layer of a metal to change the thermal profile of the part. Despite the many advancements of PCMs in thermal management systems, they have yet to be introduced and sealed in a component's surface for the purpose of reducing the effects of peak thermal loads seen by systems that generate excess thermal energy that is detrimental to their operation.

The hypothesis for this work was: the inclusion of PCM within the surface layer of a metallic component subject to transient thermal cycling will reduce peak thermal loads.

3. Background of Methods Applied to Achieve Objectives

Anodization was selected as a route to generate the PCM's host structures. The anodic layer that needs to be formed would be one that is able to accept liquid phase change material. The diameter of the porous structure formed by the anodic structure would have to be large enough and the layer will need to be thick enough to hold enough volume of PCM to effect thermal change upon the absorption of waste heat from electronic systems. This layer will need to be strong enough to withstand the various forces of the fabrication process; therefore, the nanotube walls need to be thick enough to support the PCM induction. Lastly, this anodic layer will need to be developed to survive the extreme environments that PCM materials are required to cool.

a. Mechanisms of Pore Growth by Anodization Techniques

This electrochemical process in which operating conditions such as electrolyte temperature, concentration of the electrolyte, pH of the electrolyte, the surface area ratio between the anode and the cathode, and the voltage applied play a crucial role in the morphology of the anodic oxide film. This anodic layer can be up to several micrometers thick and is formed on the anode when a current of sufficient voltage flows through the electrolyte from the cathode. The involved mobile species in the anodizing of aluminum in aqueous solutions are Al^{3+} cations, and OH^- or O^{2-} anions. The oxidation of anode at the aluminum-oxide interface generates cations, while the anions are formed at the oxide-solution interface by stripping H^+ from H_2O molecules. Ionic migration through the oxide film under a high electric field enables the growth of the oxide film. Anions migrate through the film toward the aluminum-oxide surface, and once there they react with Al^{3+} cations which results in oxide formation. At the oxide-solution interface additional alumina, Al_2O_3, will continue to form [24]. This migration of ions is shown in Figure 5 below.

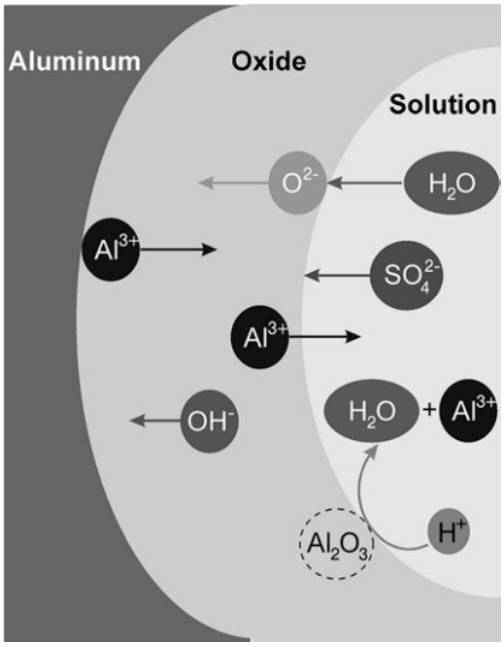

Figure 5. Ion movement and dissolution of oxide in sulfuric acid electrolyte solution. Source: [24].

If the pH of the electrolyte is neutral and has a relatively low reactivity towards the anodic film, no Al^{3+} cations are dissolved into the electrolyte. The formation of Al_2O_3 must occur for this anodic layer formation, but the electrolyte must have some reactivity towards the anodic film otherwise the porous characteristics of the anodic layer will not form [24]. The formation of the anodic layer is shown in Figure 6, and establishment of pores is shown in Figure 7.

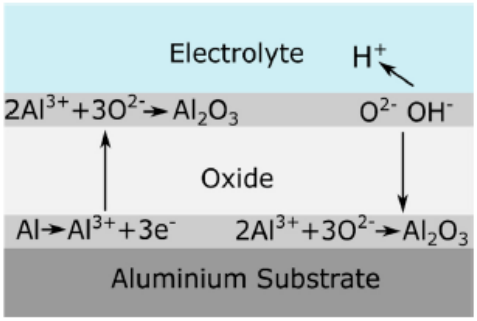

Figure 6. Ionic process during barrier oxide layer growth. Source: [24].

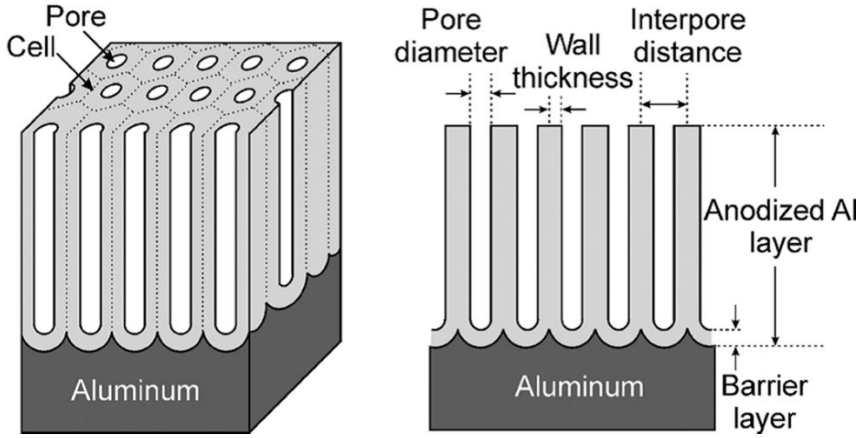

Figure 7. Ideal porous anodic oxide layer. Source: [24].

The mechanism of pore formation has been highly debated but what stands across multiple fields of study regarding the formation of the porous anodic layer are the effects of variables such as current density, temperature, electrolyte concentration, and time [24]–[27].

The work portrayed herein employed oxalic acid to create the aluminum layer because in previously reported research aluminum that was anodized with sulfuric acid held residual SO_4^{2-} ions which affected the scope of application. This problem was solved when anodizing aluminum with oxalic acid [25]. The latter showed that spacecrafts experience thermal cycling as they pass in and out of the Earth's shadow, severely affecting the surfaces and components of the spacecraft. For this reason, anodized alumina created via sulfuric and oxalic acid were compared for their stability and strength under the vacuum of space and in similar ultra-violet conditions experienced in Low Earth Orbit (LEO). After ultraviolet radiation of 1000 equivalent sun hours, the solar absorbance was significantly less for the layer generated with oxalic acid than the sulfuric acid anodic layer. The sulfuric acid layer started to crack once exposed to vacuum while the oxalic acid layer withstood the vacuum and did not start to crack until approximately 500 equivalent sun hours [28].

b. Annealing of the Anodic Layer

The annealing of amorphous aluminum oxide enhances its chemical stability; thus, annealing of the anodic layer is essential for a wide range of use cases. To improve chemical stability of the alumina layer, without affecting the structural capability of the aluminum substrate, a temperature must be selected to anneal the anodized aluminum. In a study conducted by Roslyakov et al. [29] oxalic acid generated alumina was annealed for 24 hours at varying temperatures. This study did not include the annealing of the aluminum substrate, so they were not limited by the melting temperature of raw aluminum. While they found that temperature of up to 1150 ºC will reduce most impurities and create a more crystalline anodic structures, partial decomposition of impurities begins at 450 ºC. Increasing the crystallinity of the anodic layer is critical in the contribution to anodic layer strength.

c. Phase Change Material Selection

The PCM melting temperature should be below the maximum operating temperature of the equipment that they are selected for. Their low thermal conductivity requires that they are used with high thermal conductivity materials to be effective. Aluminum that is fabricated into a geometry that allows heat exchange such as a heat sink

with fins can distribute the PCM over a large surface area, in essence, decreasing the effects of low thermal conductance [2].

Paraffin waxes such as n-eicosane, n-hexadecane, and n-octadecan have phase transition temperatures in the range of 18–35 ºC and are famous organic PCM's used for thermoregulating properties [30]. N-Eicosane was chosen for this study for its relatively high latent heat energy of 237 kJ/kg [2] and its use in previous studies in macro sized heat sinks with comparable results.

d. Vacuum Impregnation

In another study conducted by Wu at al [31], lubricant was infused in the aluminum anodic oxide (AAO) nanochannels with a depth of 50 µm by the use of vacuum impregnation. This procedure, which is commonly used in other fields of research, was effective at impregnating the anodic layer of aluminum specifically. Therefore, a vacuum impregnation system of similar construction to the one used by Wu et al. in Figure 8 was designed for this study. The only additional requirement upon this thesis' vacuum system is that it needs to withstand temperatures that would melt the PCM.

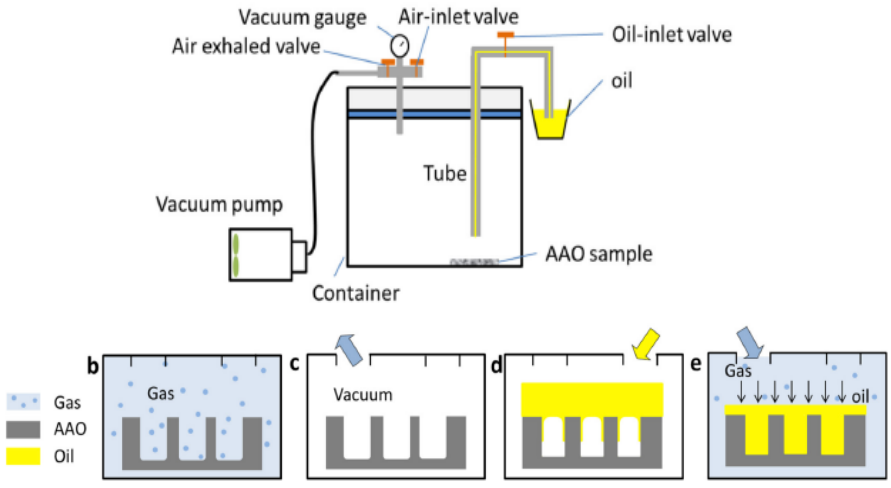

Figure 8. Vacuum impregnation aparatus and proccess of lubricant in the AAO nanochannels. Source: [31].

This process can be applied to the induction of n-eicosane wax in the anodic layer. The apparatus that is created would need to be able to withstand the heat applied during the vacuum impregnation process since the wax would need to be in liquid phase during vacuum impregnation.

e. Sealant

To ensure that the PCM impregnated anodic layer can withstand multiple thermal cycles and solid to liquid phase transitions, the PCM would need to be sealed. The two sealant methods explored in this study are epoxy and silver paint coating. Both types of coating should not leak during the solid-liquid phase transition. To accomplish this, they must be able to have their own structural integrity but must also bond to the PCM impregnated anodic layer. Past their sealing effectiveness, both methods would need to be able to have the thermal conductance to be able to affect cooling. If the sealant is too thermally insulative than the slowed rate of heating that latent heat energy storage causes during Tm, would not be observed and it cannot be said that the PCM is having an effect at preventing a heat source from causing peak cyclic loads.

C. CHAPTER OVERVIEW

This thesis is split up into the following topics: experimental methods, results and discussion, and conclusion/ next steps. The following is a summary of what each chapter will contain.

Experimental methods, introduced in chapter two, discuss the overall process of fabricating the PCM induced anodic layer. Fabrication consists of sample preparation, anodization, annealing, and coating methods. The concepts of each step have been introduced, but the methods by which they were conducted will be discussed in detail within the fabrication portion of this chapter. In addition to fabrication, testing will be discussed in this chapter as well. To prove that the PCM had an effect within the anodic structure, two separate testing apparatus were created to test the samples via Forward Looking Infra-Red (FLIR) camera and thermocouple testing. The methods of characterization are discussed in this chapter.

In chapter three, the results of characterization throughout the fabrication process are discussed and compared, when applicable, against research that also anodized aluminum in oxalic acid. The thermal data that was recorded employing FLIR and thermocouple and is shown and compared with existing literature.

Chapter four summarizes the milestones that were met as a result of the fabrication and testing steps described above. The next steps work to be done to create more uniform anodic layers without causing overgrowth. Anodic layer PCM incorporation can be further advanced through research of advanced sealants.

THIS PAGE INTENTIONALLY LEFT BLANK

II. EXPERIMENTAL METHODS

A. OVERVIEW

This chapter explains methods used to fabricate the anodized aluminum specimens that served as the porous substrates for vacuum impregnated PCM (n-eicosane) layers and the steps tp seal them. Characterization was conducted at different steps of the fabrication process to determine the effects of using diverse experimental conditions. Along with the fabrication and characterization of these samples, the chapter also discusses the testing procedures used to measure the thermal effects of the PCM once incorporated and sealed in the AAO microstructure. Figure 9 represents the steps that will be described in the sections below.

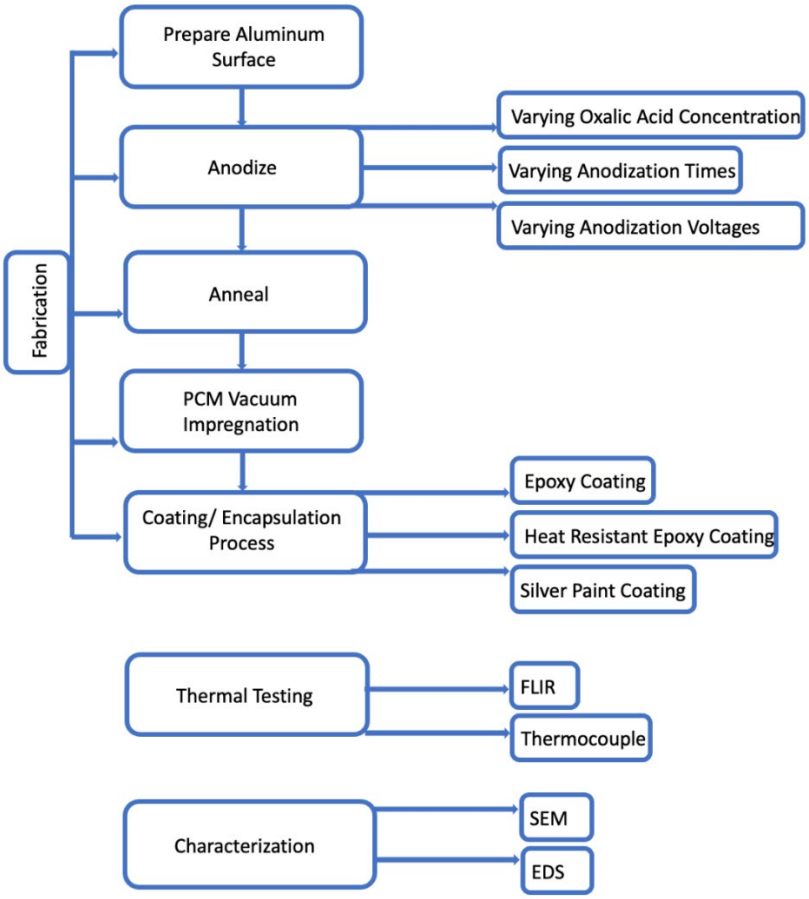

Figure 9. Flowchart of experimental methods

1. Fabrication

The component that was selected to serve as the substrate for PCM induction, was a standard, over the counter 40x40x20 mm aluminum heat sink with fins. The model selected is commonly utilized in polymeric 3D printers to cool the nozzle area. The overall goal of the fabrication steps was to apply a simple post-production process that would help improve the characteristics of an existing passive thermal management system and be able to withstand multiple transient thermal cycles. This simple fabrication process could be scaled up through application to other larger, complex parts associated with thermal dissipation.

Since the study was meant to provide a proof of concept, rather than processing the complete heat sink, individual fins were sectioned, and the surface modification was conducted on those. Figure 10 shows an overview of the fabrication process, once the aluminum fin was taken off the heat sink, from cleaning the aluminum surface to removal of the oxide layer, to producing the seal that encapsulates the anodized aluminum with a phase change material incorporated in the microstructure.

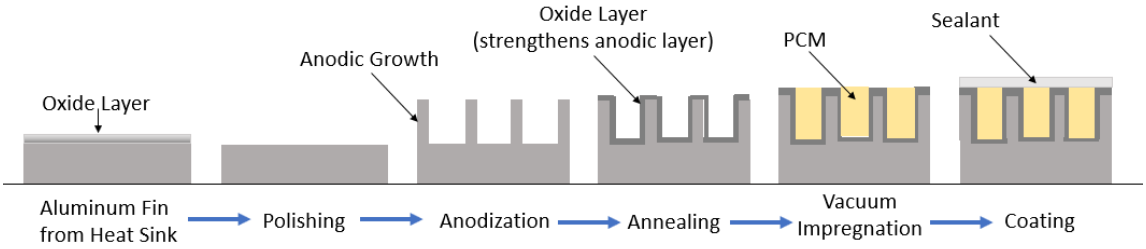

Figure 10. Fabrication overview

2. Sample Preparation

The surface of the aluminum part commercially acquired was covered by an oxide layer that needed to be removed prior to anodizing. Two different methods were selected to remove the oxide layer. The first was a chemical process which used a solution of sodium hydroxide 0.25 M (Millipore Sigma). The second was by mechanical polishing of the part itself. When the parts cleaned with the NaOH solution employed were examined under a

SEM, pitting was observed, indicating that the time employed for the process, or the concentration of the solution were higher than the ideal conditions required to remove the oxide while preserving the integrity of the metal surface. Using the samples that were cleaned in such fashion led to non-uniform growth of the anodic layer. Therefore, the primary method of preparation was polishing.

A Buehler Ecomet 4 variable speed polisher with an Automet 2 Power Head was used to polish the surface of the samples. Once the specimens were placed in Epofix resin and hardener (Struers) with curing times of 24 hours, their surfaces exposed, they were placed in an automatic polisher. Since some epoxy may have made its way on the aluminum fin surface, the first polish was for the purpose of ensuring that every surface was perfectly flush prior to fine polishing. For this first stage, P1000 silicon carbide was placed on the polisher with an RPM (rotations per minute) of 100 and the water turned on. The power head was set to 22.2 N for 10 minutes. Figure 11 shows the polishing head set up on the left and the finished product post polishing on the right.

Figure 11. Buehler Ecomet 4 set up (left), and the polished aluminum sample ready to be anodized (right)

Silicon carbide polishing disks of P1500, P2500, and P4000 were set to 5 lbs. at 100 RPM at 15, 20, and 30 minutes respectively. For the fifth step, a Buehler polishing cloth which was run at 100 RPM at a pressure of 4 lbs. for 40 minutes. A solution of 1

micron aluminum oxide powder in deionized (DI) water and regular DI water was applied to the interface of the head and the polishing pad every other five minutes for 40 minutes. All five polishing steps are outlined in Table 1. Lastly, the polishing aluminum oxide media was removed from the samples after polishing them employing a Branson 2800 series ultrasonic bath.

Table 1. Gradient polishing stages

Polishing Process					
Polishing Stage	**Polishing Disk Used**	**Pressure [N]**	**RPM**	**Wet/Dry**	**Time [minutes]**
1	P1000	22.2	100	Wet	10
2	P1500	22.2	100	Wet	15
3	P2500	22.2	100	Wet	20
4	P4000	22.2	100	Wet	30
Final Polishing Step					
Polishing Stage	**Polishing Disk Used**	**Pressure [N]**	**RPM**	**Alumina/ DI Water**	**Time [minutes]**
5.1	Buehler Polishing Cloth	17.8	100	Alumina	5
5.2	Buehler Polishing Cloth	17.8	100	DI Water	5
5.3	Buehler Polishing Cloth	17.8	100	Alumina	5
5.4	Buehler Polishing Cloth	17.8	100	DI Water	5
5.5	Buehler Polishing Cloth	17.8	100	Alumina	5
5.6	Buehler Polishing Cloth	17.8	100	DI Water	5
5.7	Buehler Polishing Cloth	17.8	100	Alumina	5
5.8	Buehler Polishing Cloth	17.8	100	DI Water	5

3. Anodization

Anodization methods adopted were similar to the study conducted by Sanz et al. [25]. That study, which conducted a parametric analysis of anodic structures generated vs. set anodization conditions, was used to determine optimized conditions herein. An optimal pore diameter that would host a PCM while on its melted state was sought after. In accordance with Figure 12, aluminum was anodized at different voltages with varying

oxalic acid concentrations and aluminum was anodized twice at fixed variables of time, temperature, acidic concentration, and voltage. Time was also chosen as a variable to modify at a fixed oxalic acid concentration of 1.6 M and a voltage of 40 V. All samples produced were analyzed in the SEM to determine the settings that rendered the largest pore volumes.

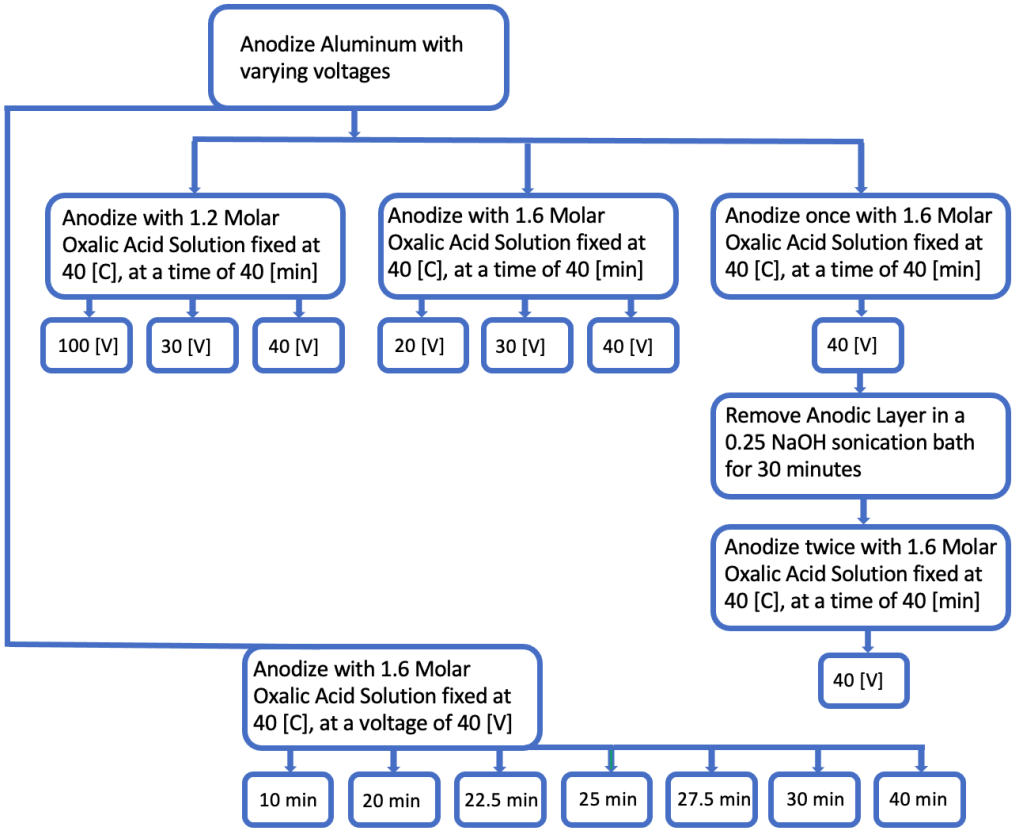

Figure 12. Anodization variables tested to produce optimal microstructures

a. Anodization Set Up

All samples were anodized with the set up shown in Figure 13. The acid used for anodization was oxalic acid dihydrate (Millipore Sigma 99.5%). An 80 ml bath of varying oxalic acid concentrations was placed on a hot plate at a temperature of 40 °C. The temperature was monitored with a mercury temperature thermometer mounted on the anodization set up. This apparatus was able to raise and lower the anode/cathode

combination out and into the oxalic acid bath. Prior to anodization, the solid oxalic acid was placed in the DI water and placed on the hot plate, with a magnetic stirrer.

The anode was placed 20 mm from the cathode in a parallel configuration. The cathode was the aluminum heat exchanger base with the fins cut off, which had a surface area that was significantly larger than that of the anode. To prepare the anode, electrical insulation tape was used to tape the back and the edges of the aluminum fin. With this method, the area of the anode was controlled to be approximately 120 mm^2 for every sample.

The DC power source (B&K Precision Model XLN15101) and digital multimeter (Keithley 2100) were placed in series and connected to metal clamps that held the anode and cathode. The positive end was connected to the anode and the negative to the cathode. The power source was programmed to a fixed voltage that slightly varied with the anodization process and set to an initial current of 0.1 A. The current was monitored at the start of every anodization process since it did not remain constant throughout the process.

Once the electrical system was initialized, the apparatus which held the anode and cathode was lowered into the oxalic acid solution ensuring that the electrical leads were not submerged. With the magnetic stirrer still running and the thermometer in the solution, a final check was done to ensure that anodization had started. The magnetic stirrer was briefly turned off to observe hydrogen bubble formation on the cathode. Once the bubbles were observed, the magnetic stirrer was turned on to an RPM that would not disturb the anode/ cathode or splash water out of the bath and onto the electrical leads.

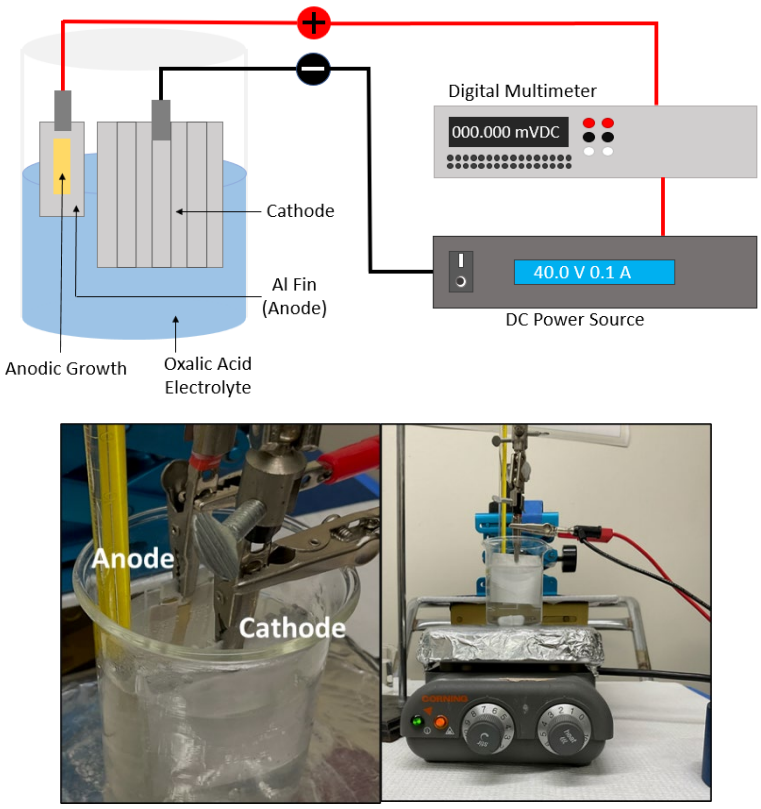

Figure 13. Anodization system and set up

b. Varying Concentration of Oxalic Acid and Voltage Applied

For the first anodization procedure, varying concentrations of oxalic acid were used at varying voltages in accordance with the second row of Figure 12. The temperature of anodization and time was fixed at 40 °C and 40 minutes respectively. The two concentrations of oxalic acid used was 1.6 M and 1.2 M. The voltages used for these concentrations were 20 V, 30 V, 40 V, and 100 V. 100 V was only used on the 1.2 M oxalic concentration. Each sample that was anodized was analyzed with an SEM.

c. Use of Secondary Anodization

At 1.6 M oxalic acid concentration, a temperature and time of 40 °C and 40 minutes similar to the procedure described above was employed to produce a specimen anodized at 40 V. This sample was then cleaned with ethanol to remove the oxalic acid solution. To remove the initial anodic layer, the sample was placed in an 80 ml bath of 0.25 M sodium

hydroxide solution and sonicated for 30 minutes. After this sample was visually inspected, it was then prepared and placed back in a 1.6 M oxalic acid solution and anodized for a second time with the same conditions that were set for the first process. This sample was characterized with SEM after being cleaned with ethanol.

d. Varying Anodization Times

The samples were prepared in accordance with the preparation procedures described above and all anodized in a 1.6 M oxalic acid solution at 40 °C and 40 V. These samples were anodized for 10, 20, 22.5, 25, 27.5, 30, and 40 minutes. All samples were then cleaned with ethanol and analyzed with the SEM.

4. Annealing

The samples chosen to be annealed were the anodized aluminum specimens fabricated at 40 °C and 40 V for 25 minutes in the 1.6 M oxalic acid solution. These were annealed using the Thermo Scientific Lindberg/Blue M Mini-Mite Tube Furnace in Figure 14. To prepare the samples, they were cleaned with ethanol then air dried after ethanol was run over the anodic surface. They were then placed in a ceramic crucible with the anodic surface face up and separated and placed in the furnace set to 500 °C for two hours. At the end of the two hours, the furnace was turned off and the samples allowed to cool.

Figure 14. Anealling crucible with sample and oven

5. Vacuum Impregnation

The vacuum chamber pictured below in Figure 15 was fabricated to induce phase change materials into the anodized and annealed aluminum fin. The vacuum chamber was made of a heat resistant Pyrex dish, a 3D printed aluminum lid with a brass pipe fitting, and a heat resistant room temperature vulcanized (RTV) silicone gasket. The gasket was JB Weld Hi-Temp RTV with a heat resistance range of 288 °C – 343 °C. The copper tube was connected to the brass fitting mounted on the aluminum lid which connected to a Buehler vacuum impregnation pump. This entire chamber was placed inside an oven with the copper pipe running out of the furnace and connected to the pump.

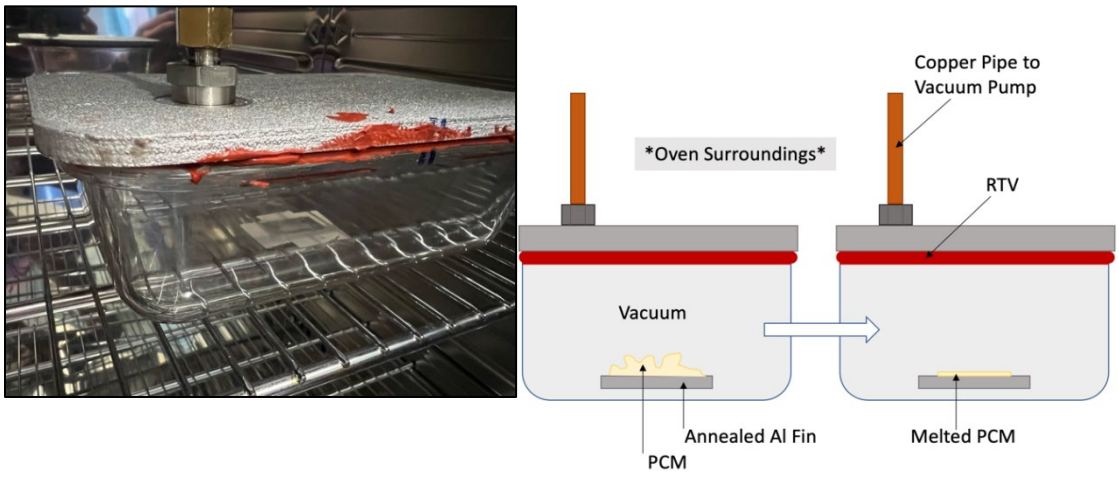

Figure 15. Heat resistant vacuum chamber

To prepare the sample, the anodic region was taped off with 3M painter's tape ensuring that the melted phase change material would remain on top of the anodic region during vacuum impregnation. The wax used as a PCM was n-Eicosane (Millipore Sigma). 0.05 g of n-Eicosane wax was measured and placed on the anodic region and evenly distributed. The sample was then positioned in the chamber as pictured above. With the aluminum lid and the copper tubing attached, the pump was turned on. The furnace door was closed, and programmed to heat to 45 °C. Once the furnace reached the set temperature, a timer started for 15 minutes. At the end, the furnace was turned off and the chamber allowed to cool while the vacuum was still applied. When the chamber reached

room temperature, the pump was turned off and the tape was removed, ensuring no phase change material was removed with the tape.

6. Encapsulation

To prevent phase change material leakage during heating, and to ensure that cooling effects of the phase change materials could be repeated, they must be sealed. To prepare each sample, the outer raw aluminum surface was washed with ethanol to ensure that all tape residue from the vacuum impregnation process had been removed. The surface was prepared by sanding with 300 grit sandpaper to ensure that the chosen sealant had a strong mechanical bond to the area surrounding the phase change material.

a. Epoxy

Two different types of epoxies were used. Struers Epofix with a 25 to 3, resin to hardener ratio by mass, and Stone Heat Resistant (HR) Epoxy with a 1 to 1 resin to hardener ratio by volume. For both types of epoxies, they were mixed with their respective mixing ratios by hand for five minutes and allowed to settle for five more minutes. To apply, a fine haired brush was used to thinly coat the entire sample, ensuring that the phase change material was completely covered. Once the fin had the uncured epoxy applied, it was placed in the same vacuum chamber used for vacuum induction of the phase change material to pull any air bubbles introduced from mixing out of the film. The vacuum was applied using the pump, and the epoxy was allowed to dry in the vacuum. The heat resistant epoxy was allowed to cure for 72 hours prior to thermal testing and the Epofix epoxy for 24 hours prior to thermal testing.

b. Silver Paint

The silver paint used as a sealant was a silver solution in Iso-Butyl Methyl Ketone (Ted Pella Inc). To distribute the silver particles prior to application, the silver paint bottle was sonicated for ten minutes. A cotton swab was used to apply the silver paint to the entire surface of the aluminum fin. Immediately after application, the aluminum fin was placed in the vacuum chamber and a vacuum was applied for thirty minutes. While the aluminum fin was drying in the vacuum chamber, the silver paint was placed in the sonication bath to

ensure that any particles displaced after the first application were again evenly distributed. After thirty minutes, a second coat of silver paint was applied to the entire surface and placed in the vacuum chamber for thirty minutes. At the end of the timer, the vacuum pump was turned off and the fin was allowed to dry for 24 hours prior to thermal testing

B. THERMAL TESTING PROCEDURE

1. FLIR Testing and Set Up

The set up for the FLIR thermal test included one hot plate, one inch of molding sand placed inside of a Pyrex dish, and a FLIR ETS320. The one-inch sand bed was placed to slow the heating rate and allow the measurement of the endothermic reaction within the phase change material. The heating and cooling cycles were run and observed with a FLIR camera. Prior to any testing, the FLIR camera was set with a working distance of 65 mm. Every test included three samples as shown in the Figure 16. Sample one and two were both anodized and sealed, but only one had incorporated PCM. These samples had the same coating, so it could be assumed that the emissivity was matched. Sample three was a solid aluminum specimen which was placed as a control to the anodic region and the PCM induced anodic region. In the FLIR Tools plus program, the region which had the phase change material was selected. Two identically sized and positioned regions were selected on the other two samples. For all samples, the averages of each region's temperature were plotted with respect to time.

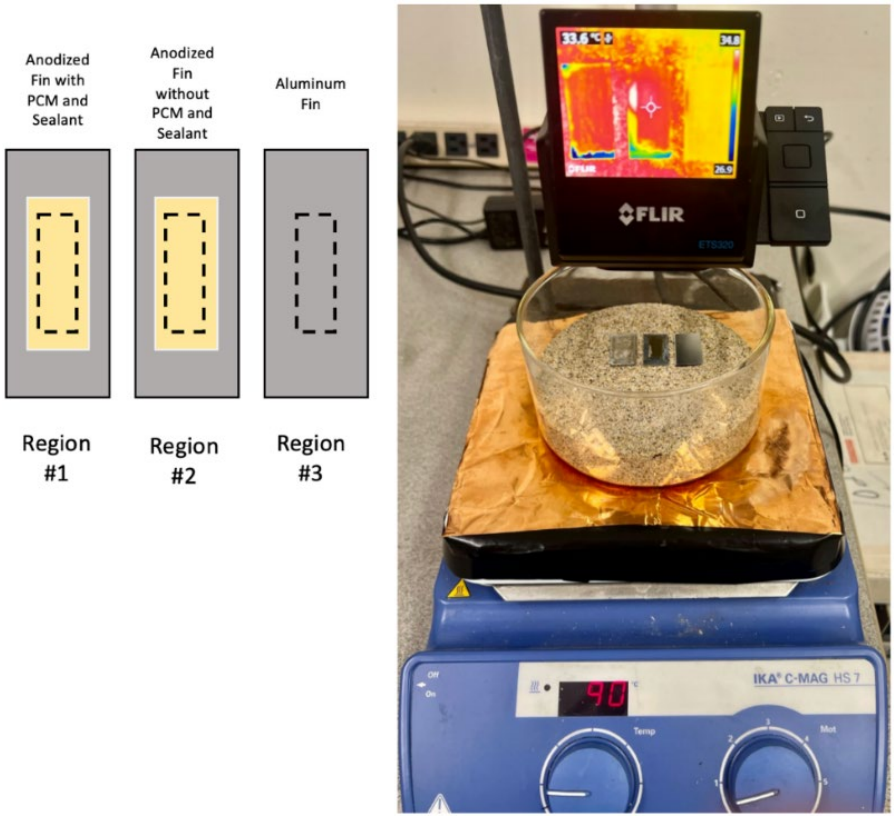

Figure 16. FLIR testing apparatus and measurement set up

The recording started at the low temperature in Table 2, the heat was turned off at the high temperature, and observation continued until the starting temperature was reached.

Table 2. FLIR thermal tests conducted

FLIR Thermal Tests Conducted					
Test	Low Temp High Temp	Melting Temperature	Phase Change Material Tested Sealant Used	Phase Change Material Tested Sealant Used	Raw Aluminum Control
ONE	30 [C]	36 [C] to 39 [C]	Anodic Layer with N-Eicosane Wax	Anodic Layer with no PCM	no anodic layer
	45 [C]		Struers Epofix Epoxy	Struers Epofix Epoxy	no sealant
TWO	30 [C]	36 [C] to 39 [C]	Anodic Layer with N-Eicosane Wax	Anodic Layer with no PCM	no anodic layer
	45 [C]		Stone Heat Resistant Epoxy	Stone Heat Resistant Epoxy	no sealant
THREE	30 [C]	36 [C] to 39 [C]	Anodic Layer with N-Eicosane Wax	Anodic Layer with no PCM	no anodic layer
	45 [C]		Ted Pella Silver Paint	Ted Pella Silver Paint	no sealant
FOUR	120 [C]	185 [C]	Anodic Layer with Lead Tin Solder	Anodic Layer with no PCM	no anodic layer
	210 [C]		Stone Heat Resistant Epoxy	Stone Heat Resistant Epoxy	no sealant

2. Thermocouple Reading and Set Up

The sand bed which was employed on the previous FLIR test was not able to be used for the thermocouple test cause the wires from the thermocouple readers lifted the aluminum surface off and caused inconsistent heating rates amongst the samples. Therefore, aluminum bars were stacked in four rows of three to in order to slow the heating rate between each row and allow a solid surface that the samples could be secured to. The specimens were placed in the same order as they had been for the FLIR tests. This set up is pictured in Figure 20. K type thermocouples were used and taped with thermally insulative tape directly on the region with the phase change material on sample one, and on the exact same position on the other two samples in accordance with Figure 17.

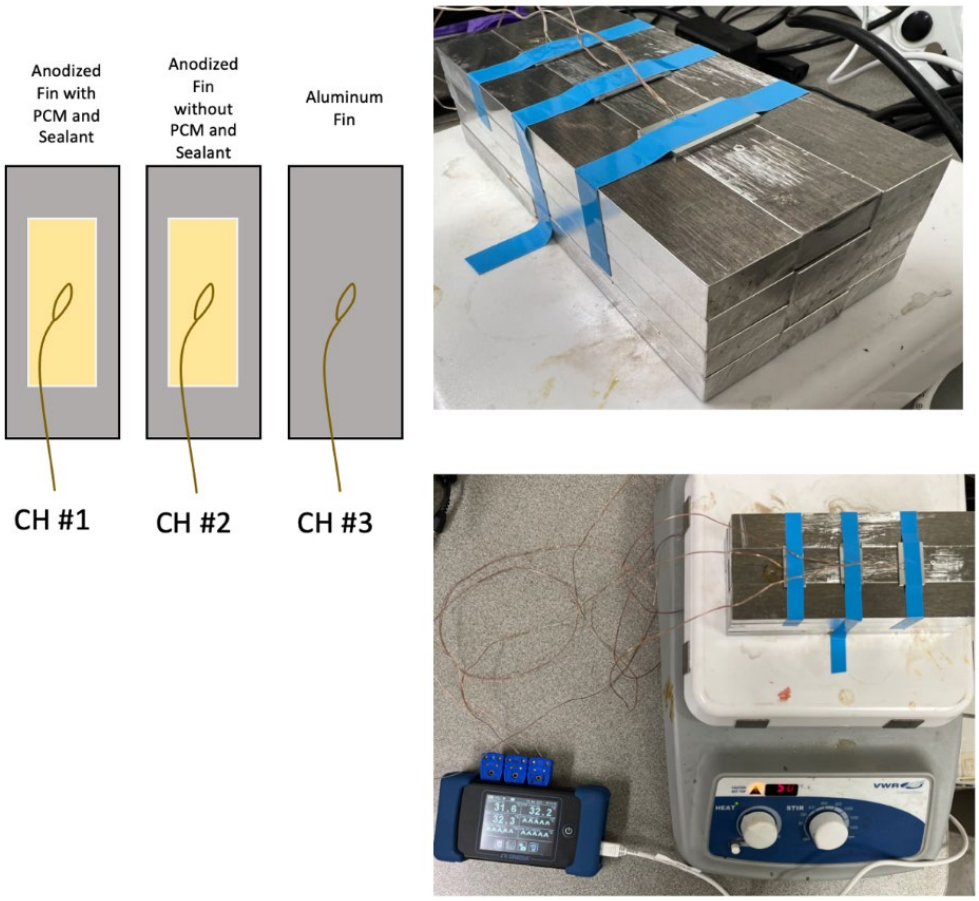

Figure 17. Thermocouple test apparatus and measurement set up

Again, the thermocouple run logs started at the low temperature indicated in the table below, the heat was turned off at the high temperature, and the apparatus was left to cool back to the low temperature before the thermocouple recording was stopped. The following runs were conducted with thermocouples as measurement devices.

Table 3. Thermocouple tests conducted

Thermocouple Tests Conducted					
Test	Low Temp / High Temp	Melting Temperature	Phase Change Material Tested / Sealant Used	Phase Change Material Tested / Sealant Used	Raw Aluminum Control
ONE	30 [C]	36 [C] to 39 [C]	Anodic Layer with N-Eicosane Wax	Anodic Layer with no PCM	no anodic layer
	45 [C]		Struers Epofix Epoxy	Struers Epofix Epoxy	no sealant
TWO	30 [C]	36 [C] to 39 [C]	Anodic Layer with N-Eicosane Wax	Anodic Layer with no PCM	no anodic layer
	45 [C]		Stone Heat Resistant Epoxy	Stone Heat Resistant Epoxy	no sealant
THREE	30 [C]	36 [C] to 39 [C]	Anodic Layer with N-Eicosane Wax	Anodic Layer with no PCM	no anodic layer
	45 [C]		Ted Pella Silver Paint	Ted Pella Silver Paint	no sealant
FOUR	120 [C]	185 [C]	Anodic Layer with Lead Tin Solder	Anodic Layer with no PCM	no anodic layer
	210 [C]		Stone Heat Resistant Epoxy	Stone Heat Resistant Epoxy	no sealant

C. CHARACTERIZATION

To understand the effects of polishing, anodization, and annealing, various methods of characterization were employed throughout the fabrication process. The characterization methods used throughout this process were Scanning Electron Microscopy (SEM) and Energy Dispersive X-Ray Spectroscopy (EDS).

1. Scanning Electron Microscopy (SEM)

Scanning Electron Microscopy was used to identify the size of the pores generated after anodic layer growth. The SEM used was the FEI Inspect f50. The voltages used to collect these images varied from a range of 5 to 20 kV to produce images at magnifications of 5kx, 10kx, 50kx, and 100kx. The working distance for all surfaces was 5 mm . For analysis of the anodic layer, samples were prepared by sputtering 3 nm of palladium on the surface of the anodic layer using a Cressington 208 High Resolution Sputter Coater. The target used for sputtering was a palladium target (Ted Pella Inc. 99.99%).

a. Anodic Region Analysis

To effectively understand the effects of changing oxalic acid concentrations, voltages, and anodization times employed, the SEM was used to analyze every anodized sample. Since these samples were only used for analysis, which would not continue through the fabrication process until verified most optimal for PCM induction, sputtering was used to prevent charging effects while studying samples under the SEM. From this analysis, the samples chosen for further production and use for PCM induction was aluminum anodized at 40 °C, with a 1.6 M Oxalic acid concentration at 40 V for 25 minutes. This sample was then recreated multiple times.

b. Cross Sectional Analysis of Anodic Region

Cross sectional analysis was done to determine the thickness of the anodic layer on the 25-minute sample previously sectioned.

c. Quality Control Analysis

SEM images were taken after polishing, anodization, and annealing for quality control. When a sample was being assessed for quality control, it was not sputtered so that it could be further advanced through the fabrication process. To prevent charging a lower voltage of 5 kV was used for imaging.

The first step of quality control started at the end of the oxide removal process prior to anodization. To ensure that the anodic structure would grow uniformly, the aluminum substrate that it would grow on would need to be as flat as possible, This provided better images that could be assessed using Image J due to uniform AAO layer growth. If the image produced poor results (scratch marks that were thicker than 2 microns), then every sample from a batch would be analyzed with the SEM and Image J, and the samples that presented large scratches were placed in the next batch for polishing.

The second step of quality control was after anodization. Since six samples were created during the polishing process, samples were anodized in batches of six. One out of every six samples were chosen for anodization.

The last step taken for quality control was after annealing. These images were taken to ensure that an oxide layer did not grow over the anodic region's pores. This could essentially shrink, or even block the pores after being impregnated with the PCM.

2. Energy Dispersive X-Ray Spectroscopy (EDS)

The Zeiss Neon 40 FESEM (Field Emission SEM) equipped with an EDAX Octane Elect Plus EDS (Energy Dispersive X-ray Spectroscopy) detector was used for elemental analysis. This analysis was done after the first anodization with oxalic acid at 40 V for 40 min at 40 °C in a 1.6 M concentrated bath. Spot EDS analysis was taken at various places on the anodic region to determine elemental composition of the thin layers created using the anodization process. For EDS analysis, the SEM was set to an accelerating voltage of 20 keV, a beam current of 1.31×10^{-6} mA, and a working distance of 5 mm.

III. RESULTS AND DISCUSSION

A. OVERVIEW

This chapter discusses results from fabrication quality assurance and characterization. SEM and raw images were collected after cleaning, polishing, and anodizing aluminum specimens. Additionally, EDS was used to characterize the anodic layer, determine the existence of oxide layer on the aluminum specimens, and if NaOH was left on the surface after cleaning. After anodization, Image J was used to analyze the porosity, pore diameter, and thickness of the AAO layer.

For thermal testing, FLIR cameras and thermocouples were used to collect data during the heat runs discussed in the previous chapter. For each run, all three samples' heat signatures were plotted with respect to time on the heating and cooling stages. The difference was plotted during the same heating and cooling cycles between the PCM induced anodic layer with the anodic layer with no PCM as well as the raw aluminum specimen prior to polishing. The goal of these thermal tests was to measure the effectiveness of the endothermic reaction during phase change of the incorporated material. This data varied with respect to the PCM used as well as the type of sealant used.

B. CHARACTERIZATION OF THE RECEIVED ALUMINUM SPECIMEN

Shown below in Figure 18 is a crosscut that was made on the surface of the aluminum specimen as received. The crosscut was made with a stainless-steel blade to analyze the material throughout the depth of the surface. Multiple EDS measurements were taken in similar regions to ensure that each elemental composition found was not an anomaly.

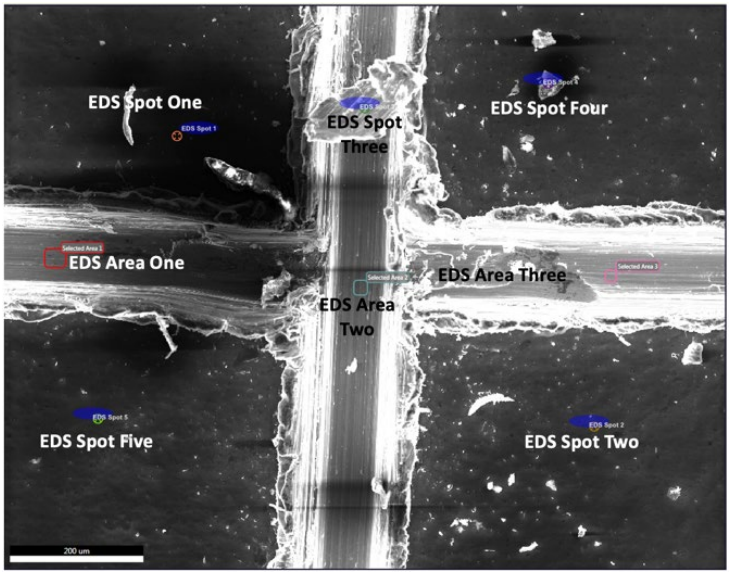

Figure 18. EDS regions analyzed

Elements found on the surface of the sample was aluminum and oxygen, while within the scratched area was just aluminum and magnesium. From these results in Figure 19, it can be concluded that the aluminum as received is alloyed with magnesium and was annealed as part of its own fabrication process. Therefore, an oxide layer is present on the part.

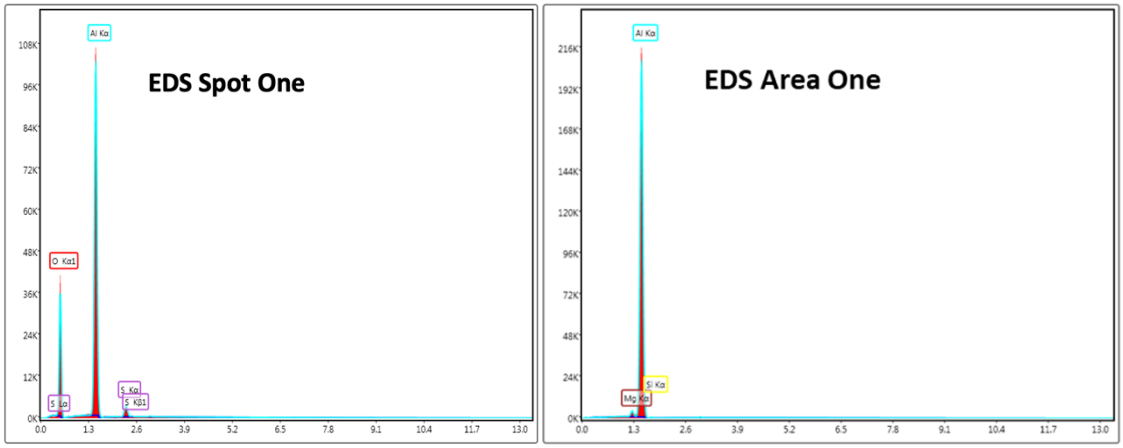

Figure 19. EDS analysis of aluminum specimens as received

C. OXIDE LAYER REMOVAL

The first method used a sonicated NaOH bath, while the other was with polishing as discussed in the experimental methods chapter. To characterize the effectiveness of this removal, EDS and SEM were used. In Figure 20, SEM pictures revealed that polishing created a much more uniformly flat layer than that of the sample that was cleaned via the sonicated NaOH bath.

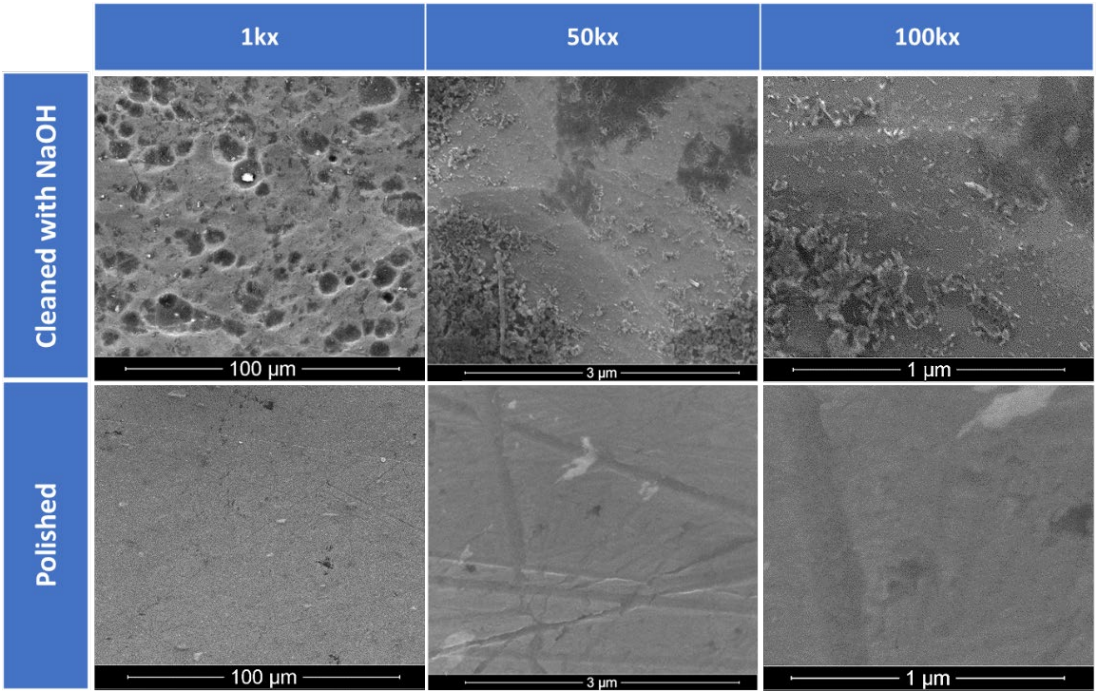

Figure 20. Oxide removal comparison between NaOH (Top Row) and polishing (Bottom Row)

When NaOH was used, it appears that the oxide layer was removed, but it also caused pitting to occur throughout numerous places on the aluminum. In addition, it also left NaOH deposits even though it was thoroughly rinsed with ethanol. These deposits were identified with EDS analysis shown in Figure 21. As done before, a blade was used to create a crosscut to analyze the surface throughout the depth of the sample.

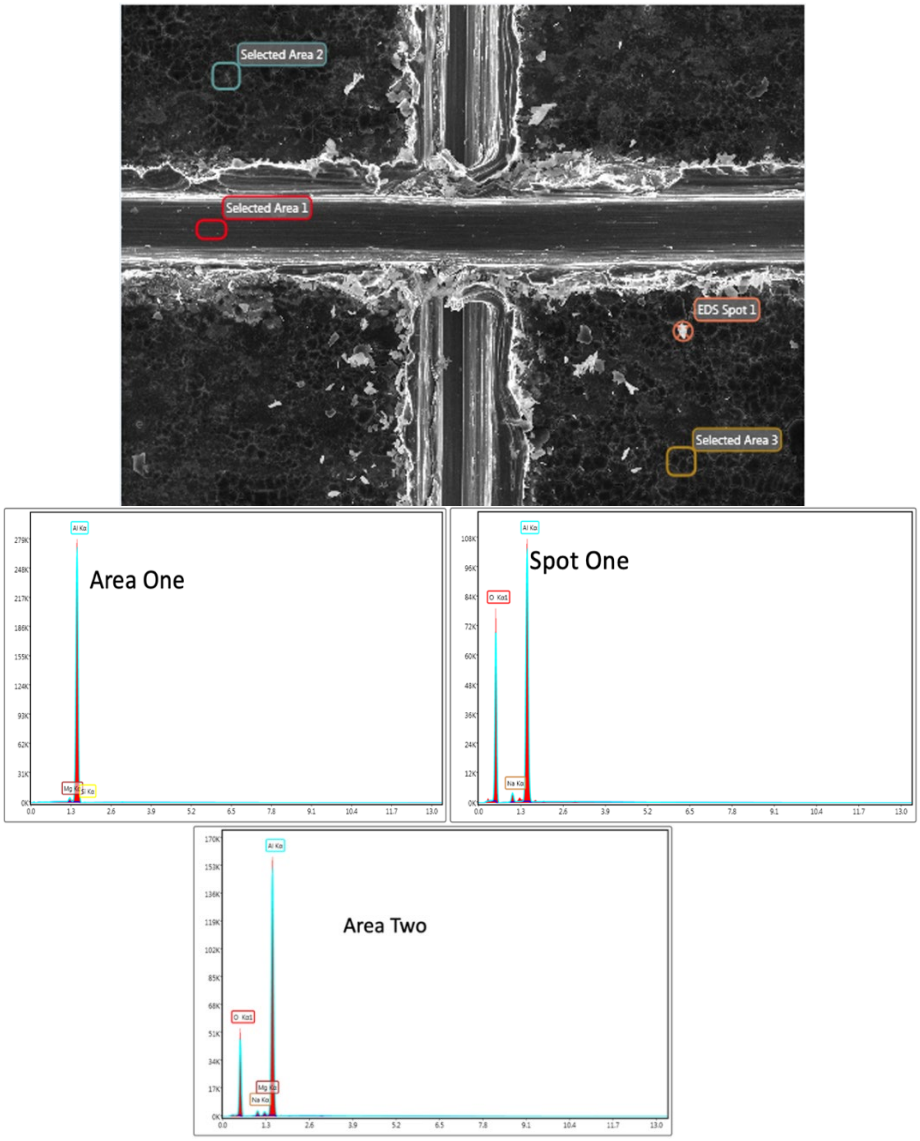

Figure 21. EDS SEM crosscut (top) and analysis of three regions

Area one in Figure 21 shows that the crosscut was able to remove not only the NaOH deposits, but also any oxide layer that may have remained. EDS analysis of spot one was done to analyze the white deposit shown on the surface of the pitted aluminum. It shows that the spot is composed mainly of aluminum, magnesium, and sodium. To further analyze the surface or determine if the white deposit was NaOH that had been left on the surface after cleaning, area two was analyzed. Area two was consistent in elemental composition with spot one, but there was no visible deposit that would have caused the

existence of oxygen and sodium compound. This oxide removal method did not remove the entire oxide layer and left deposits throughout the surface of the aluminum specimen. For this reason, polishing was chosen as the primary method of oxide layer removal.

Polishing produced mirror like results at the macro level as pictured in Figure 22 (left). The NaOH removal produced a very dull surface of aluminum pictured in Figure 22 (right). Polishing these samples was a very long process as discussed in experimental methods and would not be able to be employed on the surfaces of geometrically complex parts such as heat sinks. The biggest recommendation for manufacturers looking to employ phase change material induction is to not anneal the part until after the anodic structure has been created. Imperfect surfaces do not inhibit the growth of the anodic layer, but for the sake of this study, the surfaces were only polished to near perfection to ensure uniform growth of the AAO in order for easier analysis via Image J. Those results are discussed later in this chapter.

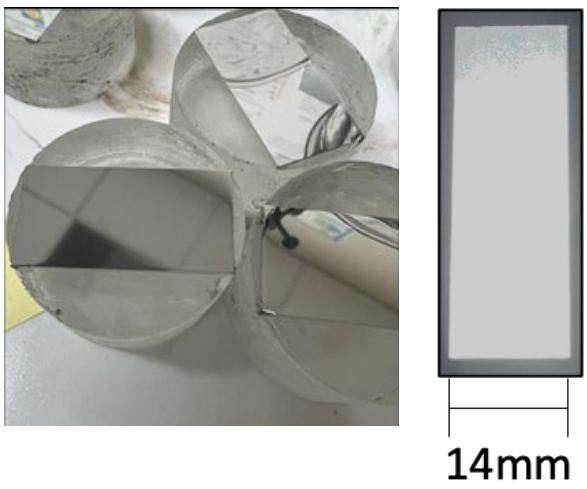

Figure 22. Macroscopic comparison of oxide removal methods

D. ANODIC STRUCTURE ANALYSIS

In accordance with previous oxalic acid anodization processes, specific variables were chosen to re-create anodic structures that would be optimal for phase change material vacuum impregnation. The goals of the anodic layer growth were to: create diameters that

were large enough to accept melted phase change materials, have cell walls that were thick enough to withstand the force applied by these fabrication processes, and have the thickness and porosity to hold enough phase change material to influence cooling. The first variables chosen to adjust were oxalic acid concentration and voltage. The results from these procedures are shown in Figure 23.

To ensure that an AAO layer was elementally composed of aluminum and oxygen only, EDS analysis was conducted of a sample that was anodized for 40 minutes at 40 °C with 40 V. This EDS analysis is shown in Figure 23 and the elemental composition of both regions analyzed contains aluminum and oxygen.

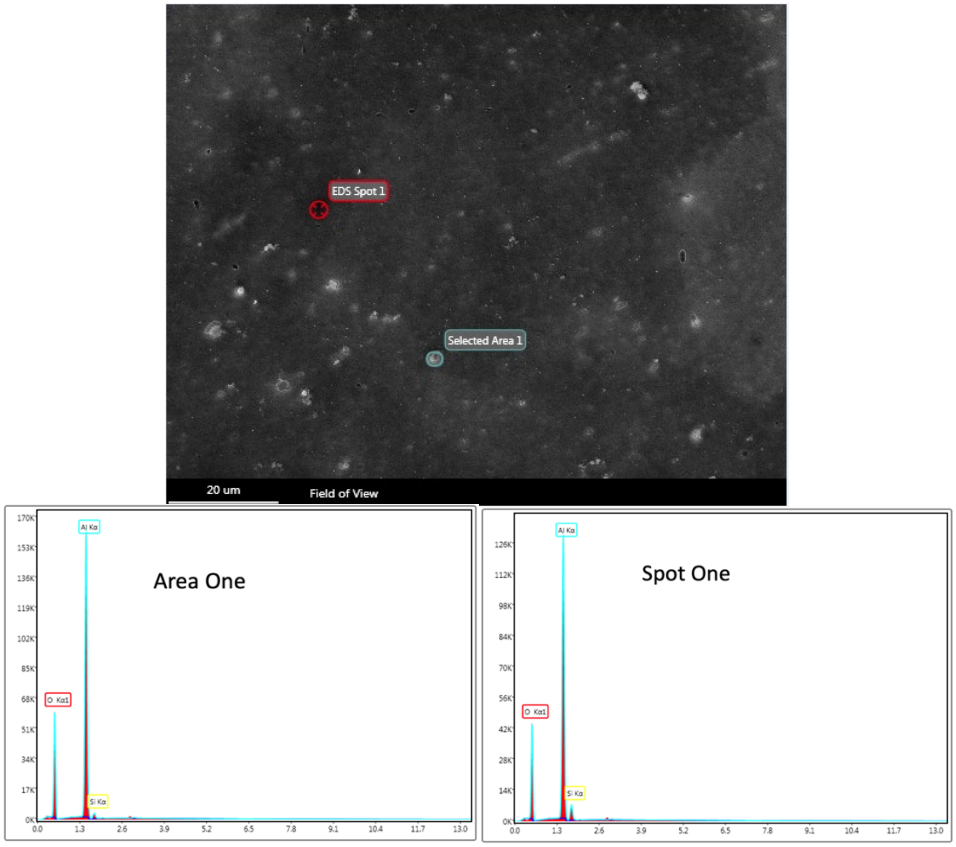

Figure 23. EDS region analysis of the anodic structure

Two regions were analyzed to ensure that the data from one region was not an anomaly. There are traces of silicon in these samples, but this could be a result of cleaning

the sample prior to SEM analysis. This sample was cleaned with ethanol in accordance with the previous chapter, but to expedite the drying process an aerosol can was used to force air over the sample and dry the ethanol.

While monitoring the electrical currents throughout the AAO growth, at higher oxalic acid concentrations there was a much steeper initial drop at the start of the process. This drop is the result of the increased resistance that is created from the growth of the anodic layer. Since the voltage is fixed, the current increases until it reaches a steady state until the indicated voltage at the start of the process is reached and them maintained. At 1.2 M, the drop was not as large as at 1.6 M concentration. Based on the pictured comparison in Figure 24 it can be concluded that the rate of growth was much faster in a higher concentration. Furthermore, concentration was the only variable that was changed amongst these images. Every sample shown was anodized at 40 V for 40 min at 40 °C in their respective concentrations. Therefore, 1.6 M concentration of oxalic acid was chosen to move forward with.

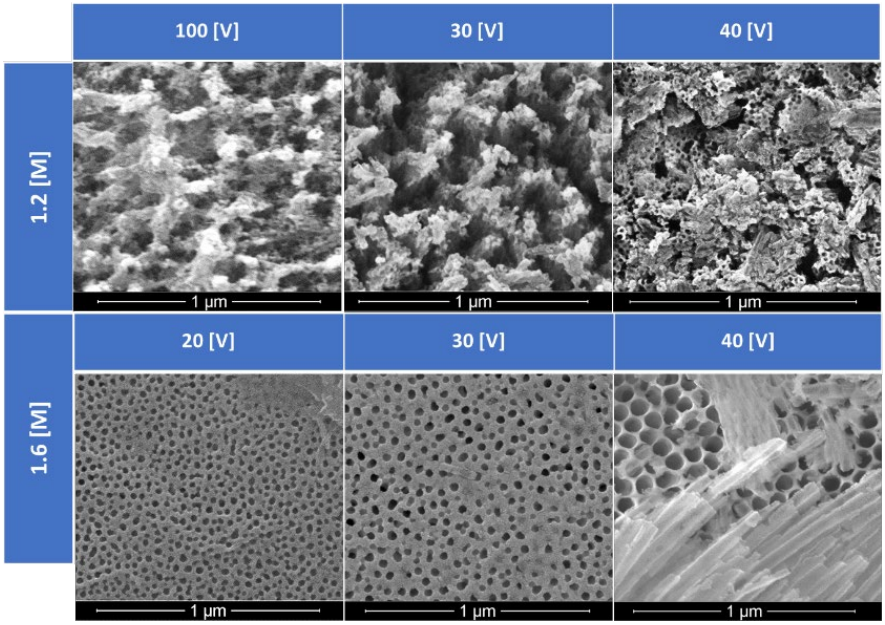

Figure 24. Oxalic acid concentration and voltage effects on the anodic structure

When looking at the oxalic acid concentration of 1.6 M, it was observed that higher voltages created larger diameter pore sizes in the anodic structure. For the application of phase change material impregnation, these larger pore sizes were preferred. Since the largest pore size shown in Figure 24 is at 40 V (pictured lower right of Figure 24). This voltage and concentration were chosen to move forward with for the anodic layer development.

The next variable that was chosen to alter was time. With the voltage and concentration of the solution fixed at 40 V and 1.6 M respectively, time would not only determine the thickness of the anodic layer, but also the porosity and diameter of the AAO layer. In Figure 25, the effects of varying time are shown. With conditions such as voltage and concentration fixed, temperature was also fixed at 40 °C. The anodization times analyzed were 10, 20, 22.5, 25, 27.5, 30, and 40 minutes.

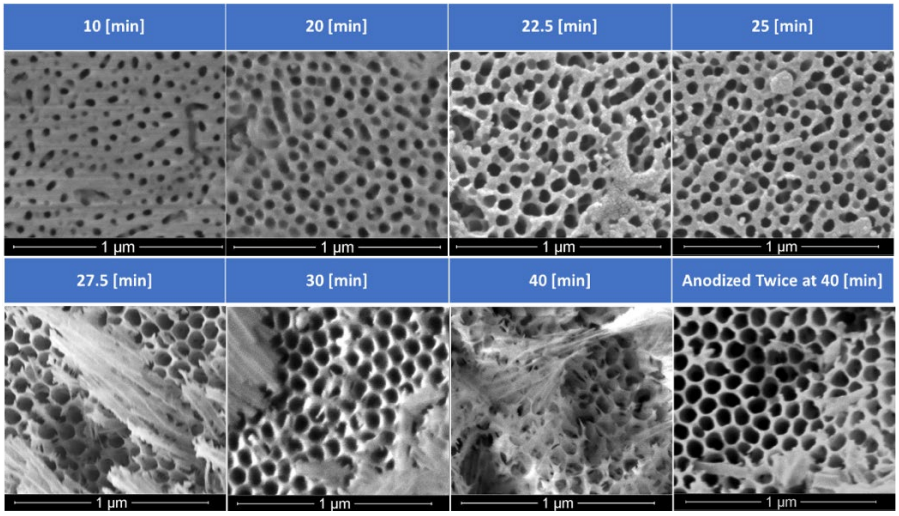

Figure 25. SEM images of AAO layer created with a variance of time

Figure 25 displays the SEM images that were taken of each sample analyzed with Image J. Even with just SEM, it is apparent that not only do the pore diameters increase, but also the number of pores per unit area.

With an increase in porosity comes a thinning of the cell walls that surround each anodic pore. Past 25 minutes, there are fibers that are visible and slightly cover each cell.

At lesser magnifications in Figure 26, these fibers shown are the development of AAO overgrowth. The overgrown layer twists and binds into its own hair like structures which blocks the anodic pores, rendering the microstructure ineffective for PCM impregnation. To try to solve this, one sample was anodized twice at 40 minutes set at the same conditions. This was done to establish a foundation for the anodic layer to grow upon and prevent the overgrowth, while providing the largest diameter pores. However, overgrowth was not prevented, therefore, the twice anodized sample was not analyzed in Image J as it was not selected for further use.

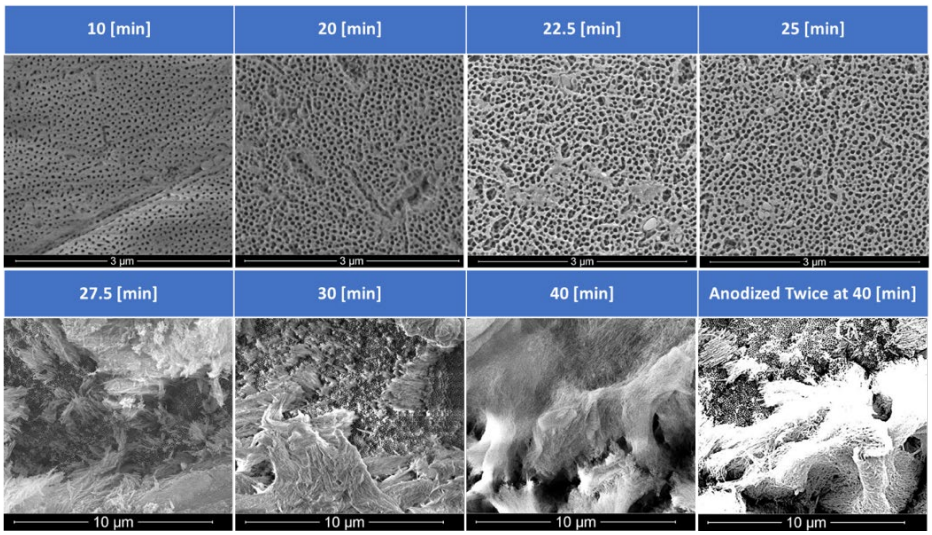

Figure 26. Development of the overgrowth in the AAO layer

To determine which conditions would be set for AAO development for every sample that would be later employed with PCM, Image J analysis was done to determine the diameters of nanotube pores. This data is shown in Figures 27, 28, and 29. When time is increased, the diameters of the pores within the AAO layer become larger. For PCM incorporation larger pores were preferred, but the AAO overgrowth was detrimental to the induction of PCM. Therefore, the time chosen was one that would drive AAO diameter to be as large as possible without causing overgrowth.

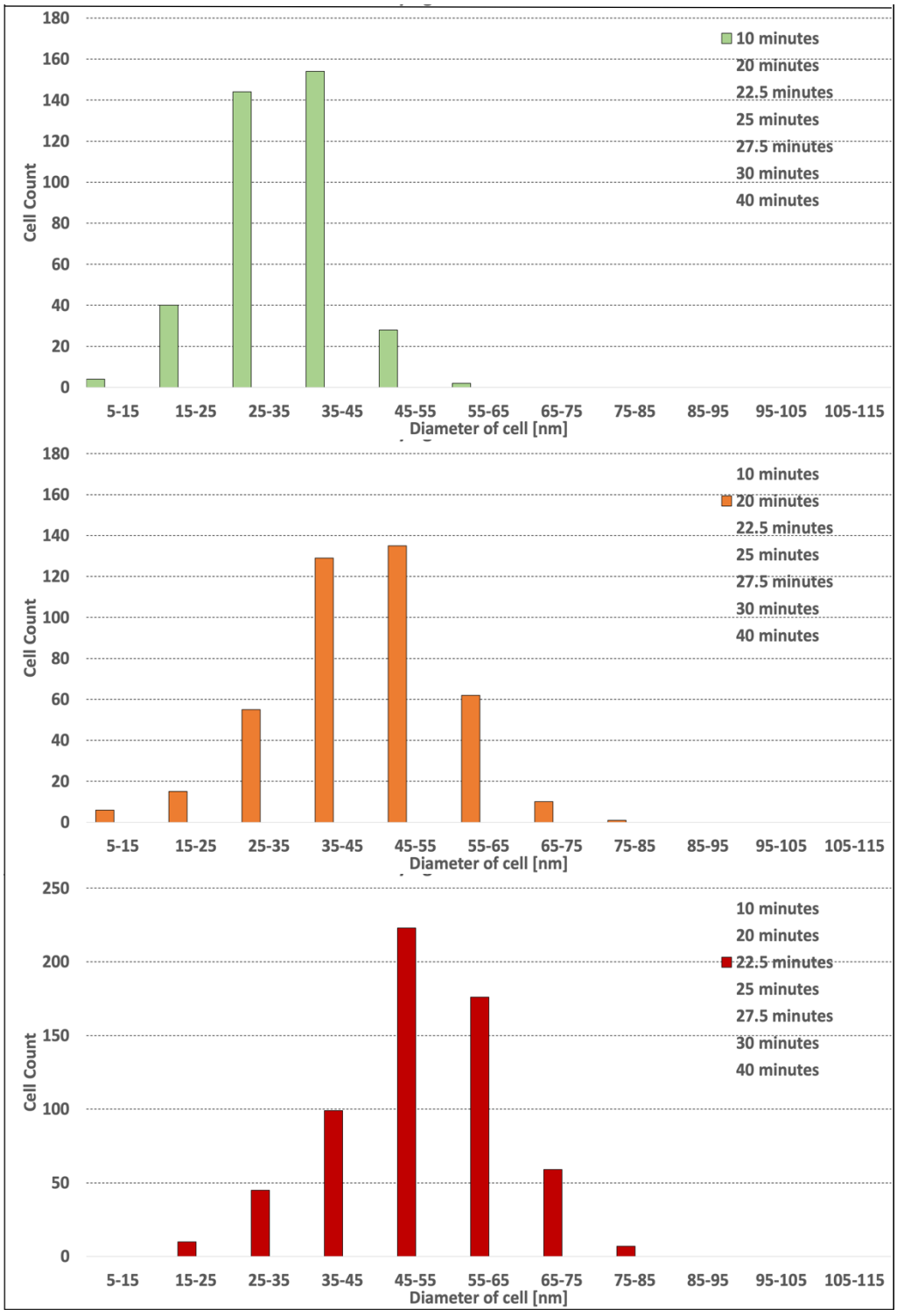

Figure 27. Effects of time on the porosity and diamter of pores within the AAO Layer 10, 20, and 22.5 minutes

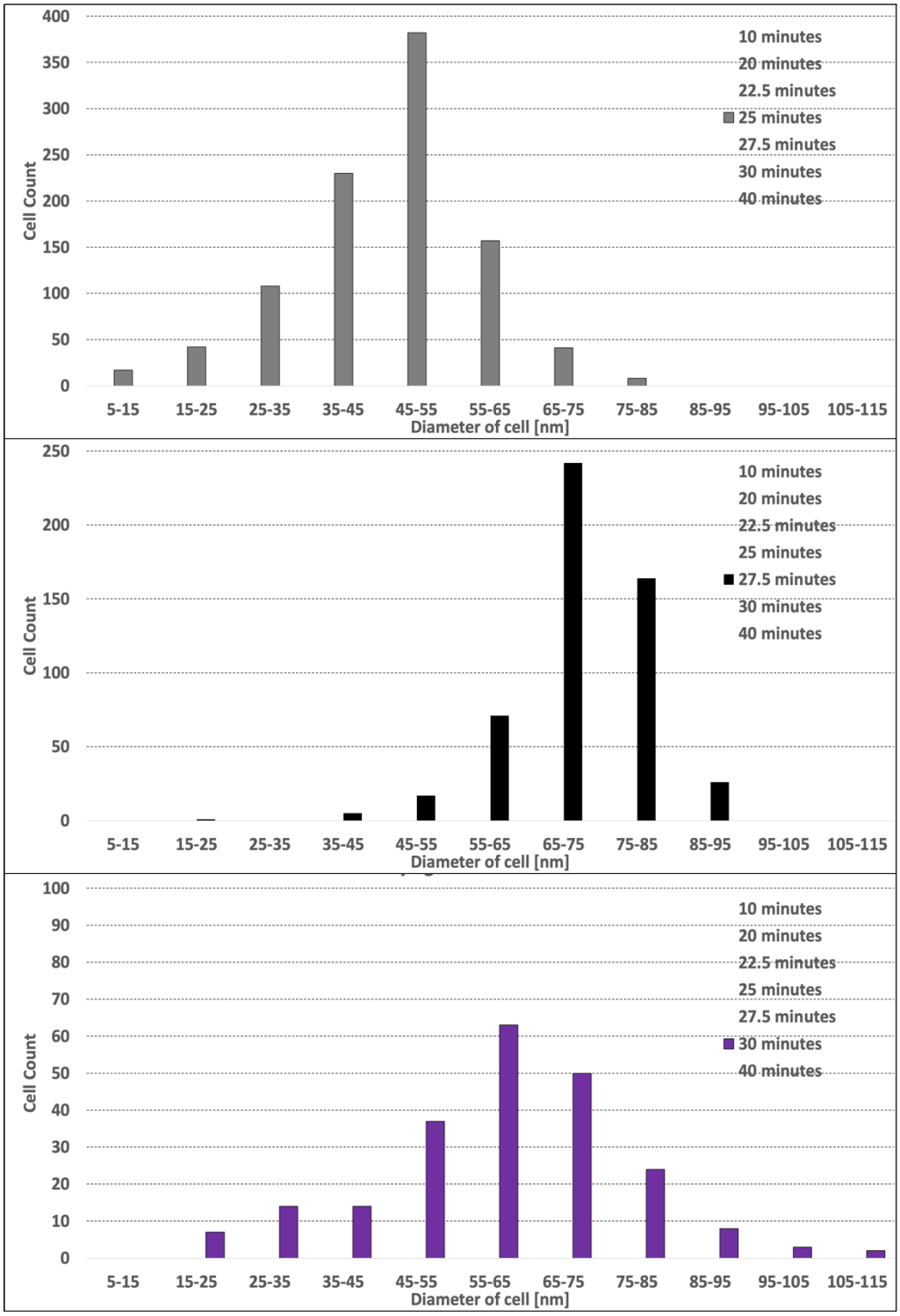

Figure 28. Effects of time on the porosity and diamter of pores within the AAO Layer 25, 27.5 and 30 minutes

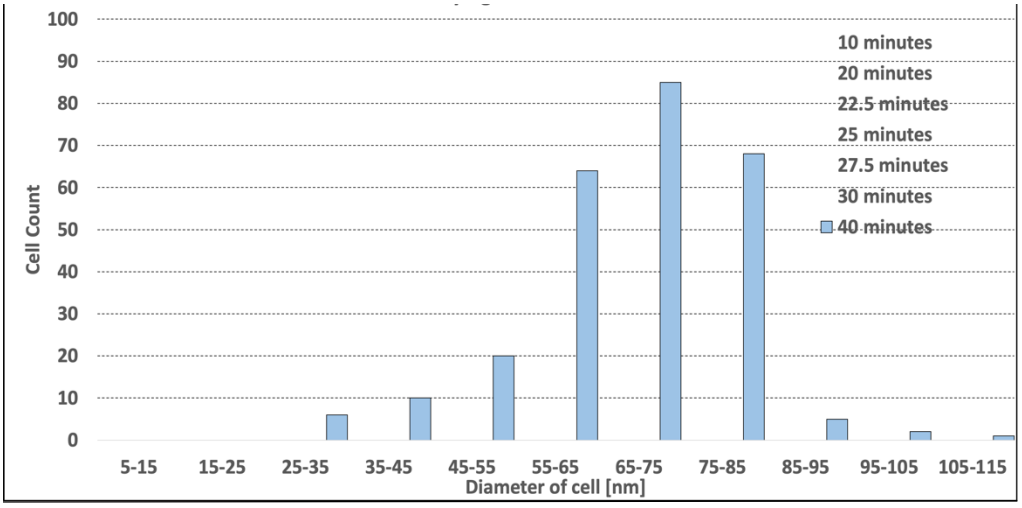

Figure 29. Effects of time on the porosity and diamter of pores within the AAO Layer 40 minutes

Changing the time to 25 minutes would create the largest diameter pore size without overgrowth and generate the thickest usable layer. Since the anodic layer continues to grow as time was increased, an SEM image was only taken of the cross section of the 25-minute sample. The cross section is pictured in Figure 30 with its analyzed thickness which was measured in Image J.

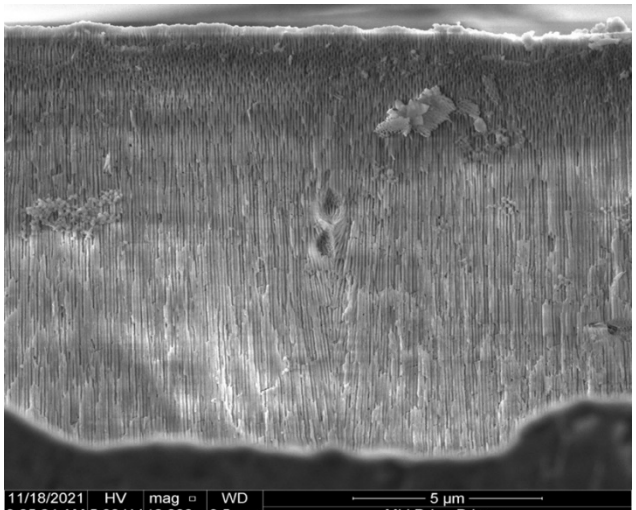

Anodic Layer Thickness

Measurements Taken	Average [nm]	Standard Deviation [nm]
100	11994.69	638.14

Figure 30. Cross section analysis and SEM images

1. AAO Discussion

Comparing these results with studies done in the past with AAO structures produced with oxalic acid, it is clear that there is a line between which overgrowth occurs and pore size is large and desirable for PCM use. As temperature, current density, and electrolyte concentration increase, the rate at which these pores form is increased. As time continues to advance, the formation of the anodic layer becomes thicker, while the diameters of the pores will continue to grow larger.

These pores will eventually experience overgrowth or chalking. Chalking is due to a chemical attack at the outer part of the oxide film which thins the pore walls and causes their upper regions to lose structural stability and collapse [24]. In a study conducted by Sanz et al. [25] the cross section of the overgrown pore layer was analyzed. An evolution of pore growth in oxalic acid is shown in Figure 31 with respect to time. Pores are formed during aluminum anodization until their layer coats the metal surface and resemble Figure 31A. This growth will continue until the walls are thinned out and the pre diameter is almost equal to that of the cell in Figure 31B. Eventually, the diameter of the pores will become higher than the cell size creating alumina fiber-like structures at the intersection points of the three cells shown in Figure 31C [25]. These fibers are the overgrowth or chalking that is created in the anodic layer.

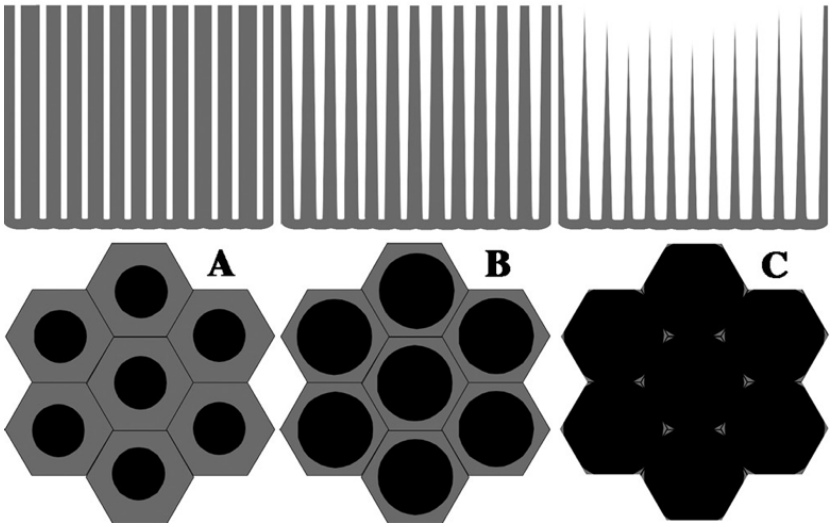

Figure 31. Images of the evolution of the AAO pore. Source: [25].

Sanz et al. concluded that by increasing the time of anodization, pore growth will continue to occur. The fibers that are developed from the pore walls coalesce and form fiber bunches shown in Figure 32.

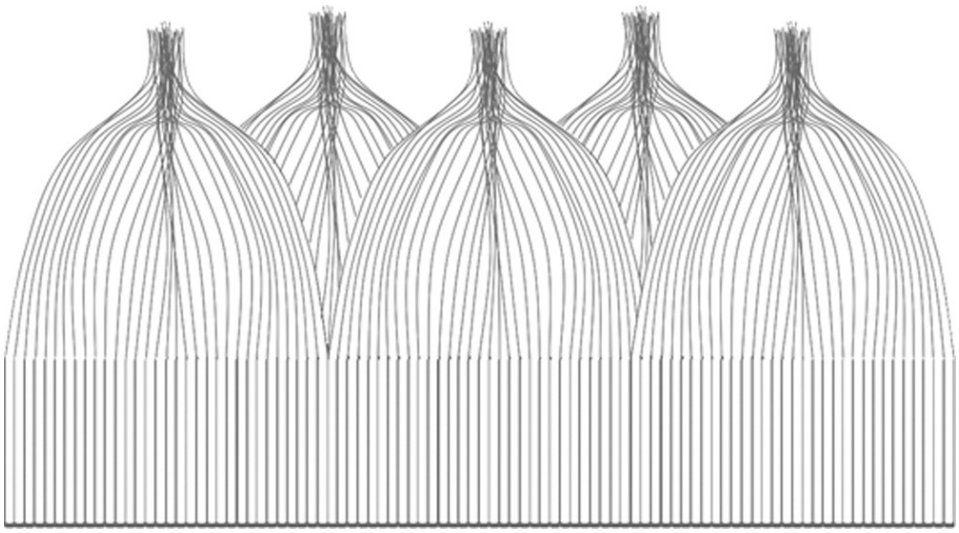

Figure 32. Lateral view of overgrown and cracked pores. Source: [25].

In order to create highly organized anodic layers, it is clear that adding more time to the anodic process is not the most effective path. Additionally, it is very difficult to get consistent results at the time when pore diameter is at its largest without pore over growth. Therefore, 25 minutes was selected to create a repeatable process that could generate large enough pore diameters.

E. THERMAL TESTING

The PCM tested was n-eicosane wax with a melting temperature range of 36–39 °C. While this wax was impregnated in the same anodic structure using the methods describe in previous sections, different sealing techniques were used. The first sealant tested was Struers Epofix Epoxy which is indicated as stable under normal ambient temperature conditions of 25 ºC. The second sealant used was a Heat Resistant (HR) Epoxy manufactured by Stone Coat Countertops. This epoxy was rated to 232 °C, which is well above the melting temperature of n-Eicosane Wax. The last sealant used was Silver Paint

manufactured by Ted Pella Inc. This Silver paint, which is comprised of a silver particle solution of Iso-Butyl Methyl Ketone was applied twice to the n-Eicosane impregnated anodic structure.

N-eicosane was thermally cycled with the respective sealants and compared with an anodic layer that was sealed without the PCM as well as bare aluminum. Each test was run twice with a FLIR Camera, and then again with a k-type thermocouple. For all tests, temperature with respect to time in seconds was plotted for all three samples simultaneously. Two additional analysis plots were created: a comparison of the PCM induced sample with its respective coating vs. an anodic layer with no PCM and the same coating, and a comparison of the PCM induced sample with raw aluminum. For each test, the heating and cooling effects were plotted. The results from the six separate thermal tests are graphed below.

1. N-Eicosane PCM with an Epofix Epoxy Sealant

The first test run was conducted with n-Eicosane Wax coated with Epofix Epoxy. In Figure 33, it is apparent that the phase change induced sample experienced an endothermic reaction from melting, and an exothermic reaction while transitioning back to solid during the cooling phase. Upon heating, this endothermic reaction slowed the rate of heating to a significant amount. This effect lasted for approximately 4.88 minutes starting at a temperature of 37.06 °C and ending at a temperature of 39.02 °C. This resulted in a maximum temperature difference of 2.27 °C when compared with the anodic layer with an epofix epoxy coat, and a maximum temperature difference of 1 °C when compared with raw aluminum. The amount of n-Eicosane spread over 120 mm^2 was 0.05 g to produce this effect. Upon cooling, the exothermic reaction peaked at 36.96 °C which is below the lower bounds of the PCM liquid phase transition temperature.

While these results measured with the FLIR camera presented endothermic and exothermic peaks, it was observed that n-Eicosane wax leaked. To produce another test for thermocouple measurement, a separate sample had to be made using the exact same parameters and n-Eicosane amounts as this first sample. A thicker layer would have

prevented leakage, however, the low thermal conductivity of the epoxy would have reduced the thermal signature of the PCM.

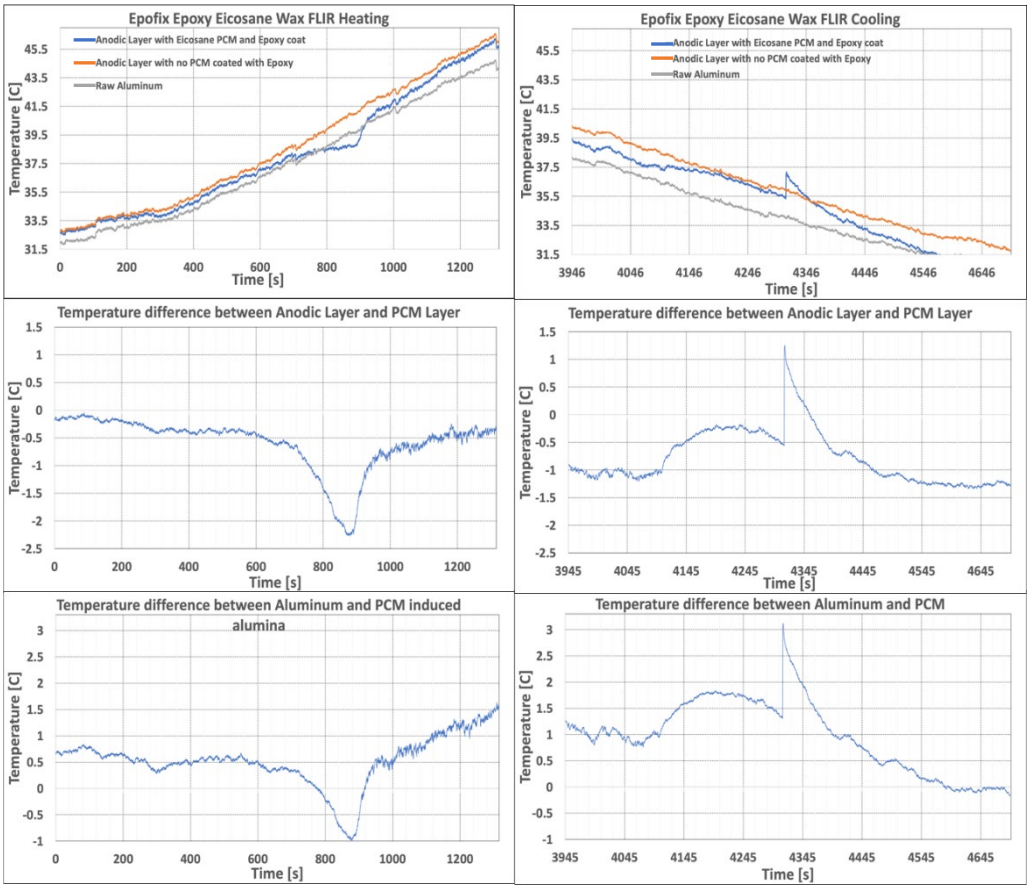

Figure 33. N-Eicosane PCM sealed with Epofix Epoxy FLIR thermal test

The second test conducted was measured with thermocouples to attempt to gain a more accurate reading of temperature. Those results are shown in Figure 34. Again, the wax leaked out of the Epofix Epoxy, producing delamination of the sealant and prevented an accurate reading. With the FLIR Thermal Camera measurement, there was an area that was observed and plotted in the FLIR Tools plus software. In the case of the thermocouples, a single point was measured using k-type thermocouples and thermal tape. It could be concluded that when the wax leaked out of the anodic structure, the thermocouple was not in the vicinity of the wax and therefore did not see the effects of the endothermic reaction. Since the wax could have leaked away from the thermocouple location, the endothermic

reaction that was observed in the previous test, was not able to be observed in this test as well. Shown only in Figure 34 are the temperature values vs. seconds because the difference between samples did not reveal any new information. Throughout the test, the thermocouple read a slightly lower value for the PCM induced sample, but this could be accounted for the fact that the wax and the epoxy together would create a thicker sample which would lead to a slower rate of heating than the other two samples that were compared.

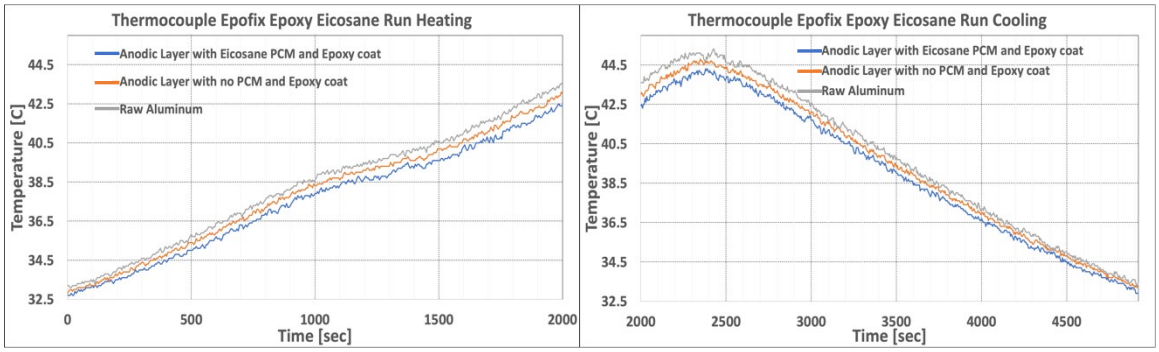

Figure 34. N-Eicosane PCM sealed with Epofix Epoxy thermocouple test

2. N-Eicosane PCM with a Silver Paint Sealant

Shown in in Figure 35, the third test run was done with the same PCM as before but sealed with two thin coats of silver paint. This test produced a similar cooling effect, and while not as dramatic as the first run, the silver paint coating was able to contain the PCM upon heating and cooling. Therefore, this coating provided promising results regarding repeatability. The FLIR thermal test is shown below with a lowered heating rate for approximately 7.11 minutes starting at a temperature of 29.83 °C and ending at a temperature of 34.89 °C. The maximum relative temperature difference 1.63 °C when compared with the anodic layer with the silver coat, and a maximum temperature difference of 3.35 °C when compared with raw aluminum. These temperature differences were observed during the heating cycle, although, the exothermic reaction effects were not observed, there was almost an acceleration of cooling that occurred with the PCM induced sample when compared with the other two. This resulted in a maximum temperature

difference for the entire heating and cooling cycle of 2.18 °C when compared with the anodic layer with the silver coat, and a maximum temperature difference of 4.56 °C when compared with raw aluminum.

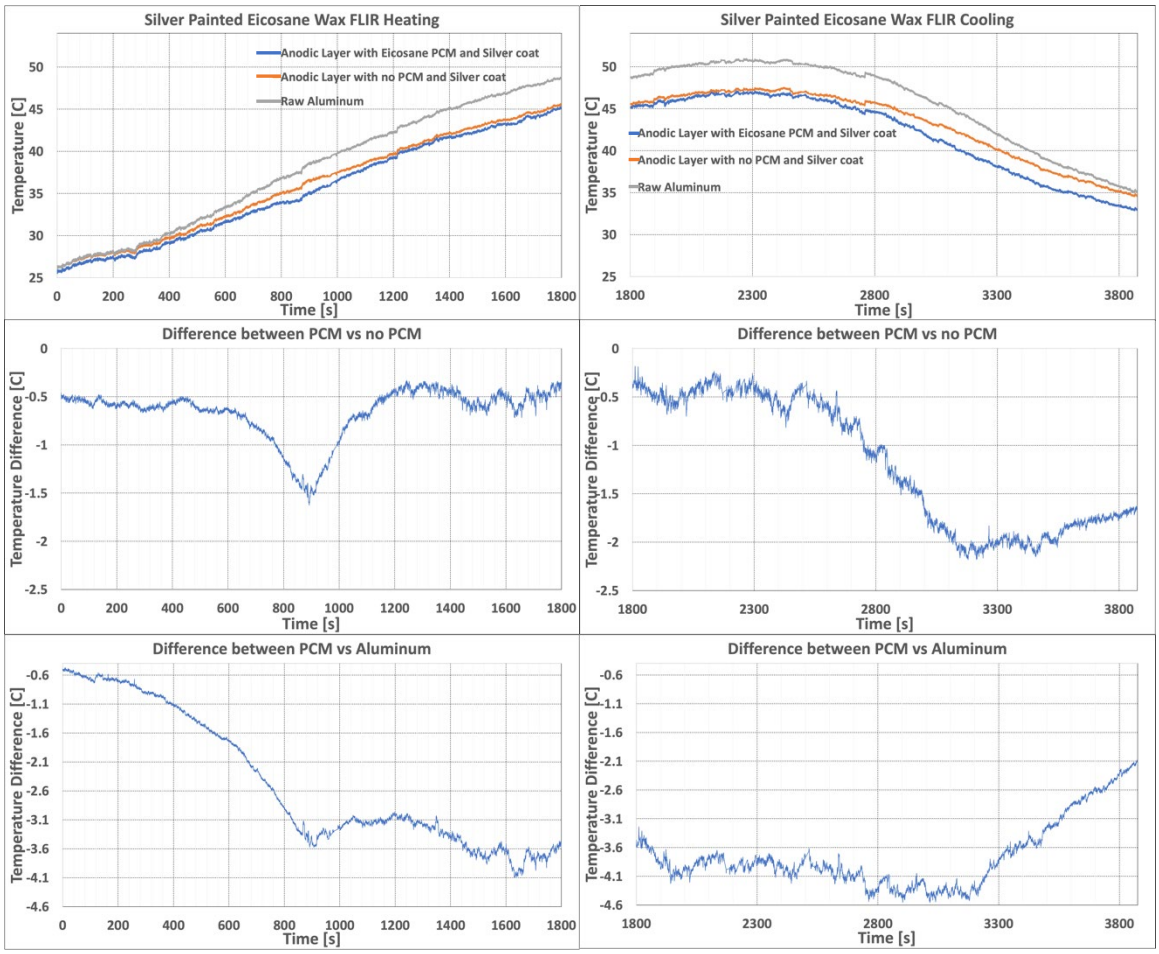

Figure 35. N-Eicosane PCM sealed with silver paint FLIR thermal test

The same specimen sealed with silver paint was used for the thermocouple test shown in Figure 36. In addition, when the thermal tape was removed from the surface of the sample, the sealant did not delaminate. The temperature difference between the anodic layer induced with the PCM, and the anodic layer without was measured at a max difference of 1.2 °C. This slow rate of heating during temperature range of 33.6-39.2 °C lasted for approximately 8.58 minutes. The temperature of the PCM induced sample was warmer than the aluminum fin throughout the heating process which was not optimal.

Like the FLIR test for the same sample, this measured an increased rate of cooling with the PCM induced sample. In addition, the solidification of the PCM was observed at 33.5 °C and rapidly peaked to 34.1 °C, which slightly exceeded the lower limit of T_m. While cooling, a maximum difference of 5.1 °C and 5.9 ºC was measured between the anodic layer and raw aluminum sample respectively.

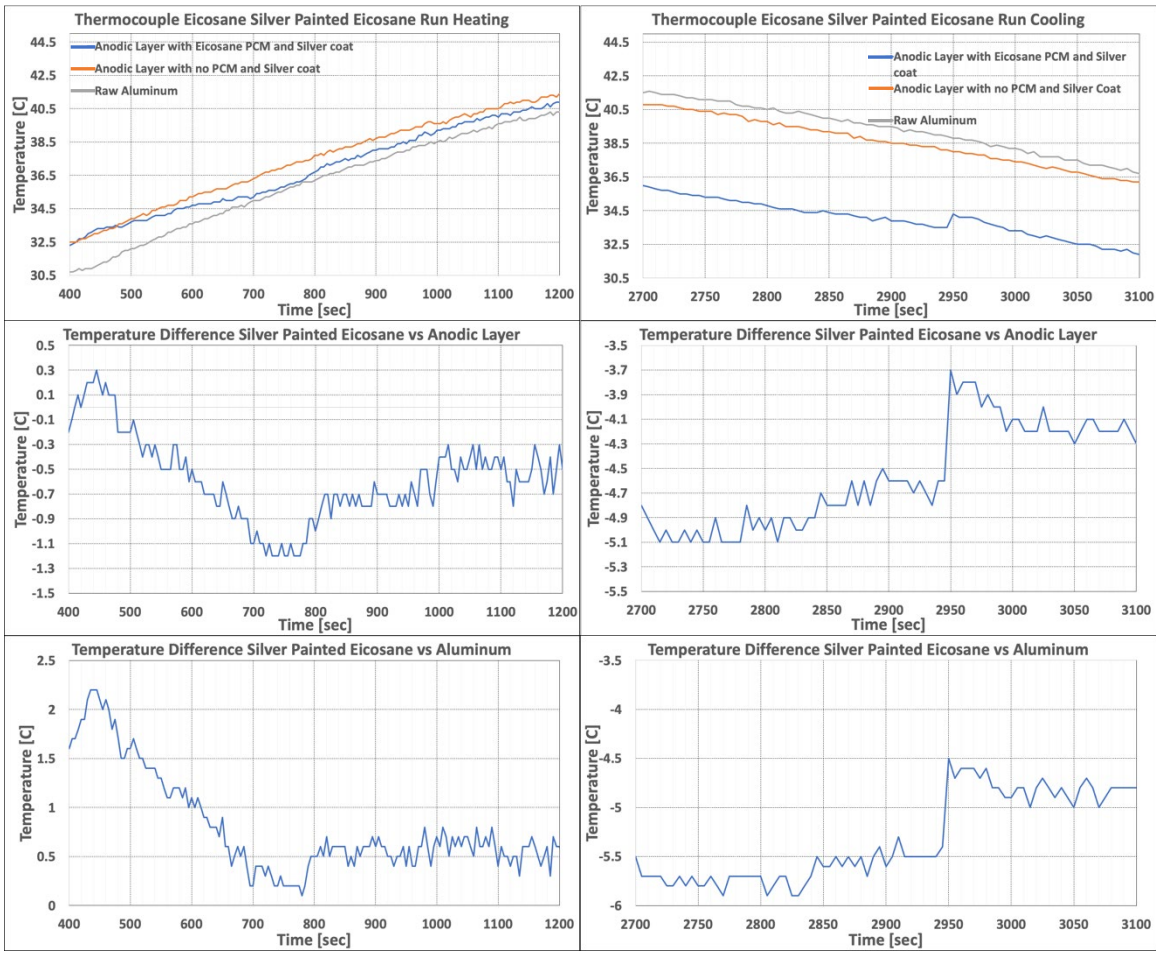

Figure 36. N-Eicosane PCM sealed with silver paint thermocouple test

3. N-Eicosane PCM with Stone Coat Epoxy Sealant

To contrast the results previously observed with those of a heat resistant epoxy sealant, the data presented below was collected. Upon heating and cooling there was no leakage, and the epoxy produced a consistently thin layer across the surface of the PCM

and the raw aluminum region, but the data from the FLIR camera measurements in Figure 37 do not reflect temperature differences between the samples containing PCM and those employed without it. Upon heating, there was no observation of a slower heating rate through the temperatures of 36–39 °C. However, an accelerated rate of cooling was identified. The maximum temperature difference measured between the PCM sample, and the anodized region with no PCM showed that the former was 2.05 °C cooler.

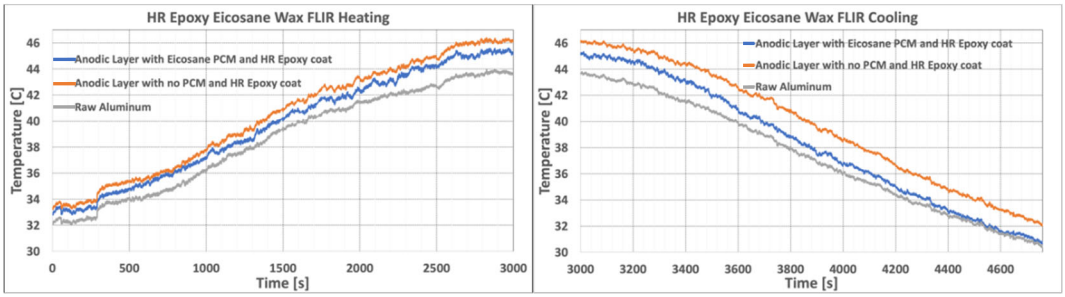

Figure 37. N-Eicosane PCM sealed with HR Epoxy FLIR thermal test

Similar results were observed when thermocouples were employed. These results from heating and cooling are shown in Figure 38.

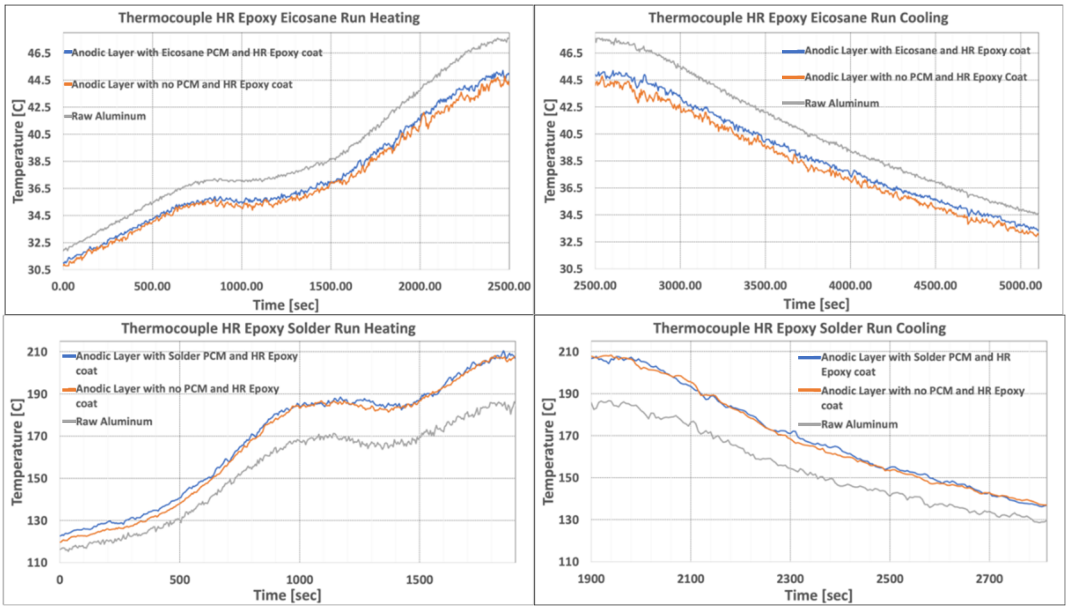

Figure 38. N-Eicosane PCM sealed with HR Epoxy thermocouple test

4. Thermal Data Discussion

To compare the results from this research with others in the literature, the study by Baby et al. [2] is presented below. In that study, PCM was incorporated within various designs of heat sinks. The three designs were a no fin compartment, a three-plate fin compartment, and 72 pin fin compartment, all made of aluminum. All three designs were tested against a heat source that would replicate the load applied by small electronic chips. Figure 39 shows a schematic of the no heat sink compartment with thermocouple placement (left), the three finned heat sink compartment (middle), and the 72 pin heat sink (right). All heat sinks had the same cross sectional area of 80 x 62 mm^2 base with a height of 25 mm [2].

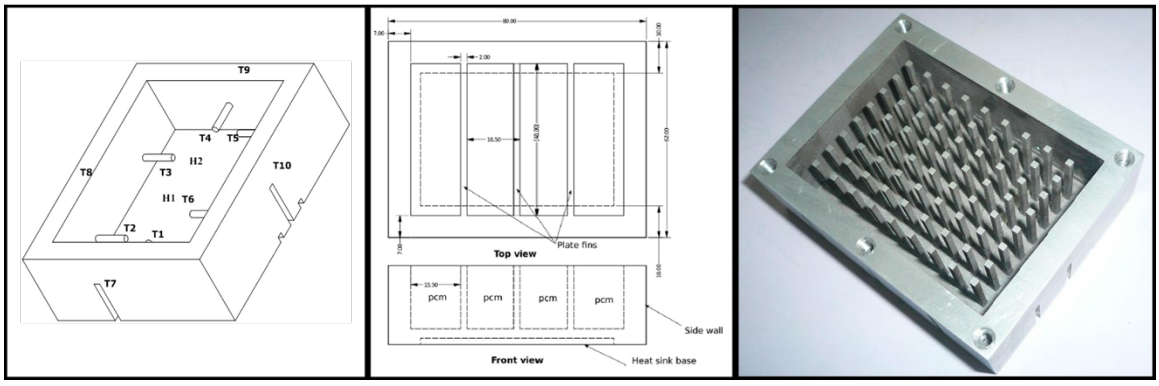

Figure 39. PCM heat sink compartments. Source: [2].

These heat sinks were sealed with an aluminum gasket, and tested while heated via a power source. The heat sink without fins had the smallest latent heat energy storage than those with fins. The largest measured energy storage was in the design with the pin fins. The set temperature for these heat sinks was 45 ºC at a power of 7 W [2]. While the objective of their study was not to measure the effectiveness of a phase change material, they did measure the temperature difference with respect to time of a heat sink which contained PCM, and a heat sink that did not contain it. Due to the latent heat of the n-eicosane PCM, it took 165 minutes for the heat sink with the PCM to reach a set temperature of 58 ºC while the heat sink without the PCM took 64 minutes. The plot of this experiment is shown in Figure 40.

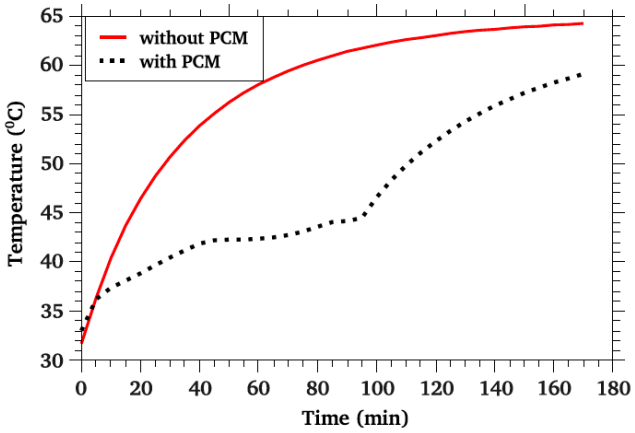

Figure 40. Temperature of heat sink with and without PCM at 4 W. Source: [2].

The maximum temperature difference between the heat sink with PCM vs. the heat sink without was approximately 17.8 ºC. The effective cooling time of the PCM significantly increased as the surface area in contact with the amount of PCM increased. Out of the three models tested, the model with 72 pin fins which were evenly distributed throughout a volume of 59.5 cm^3 filled with n-eicosane took longer to heat across all applied heating rates. These tests are shown in Figure 41.

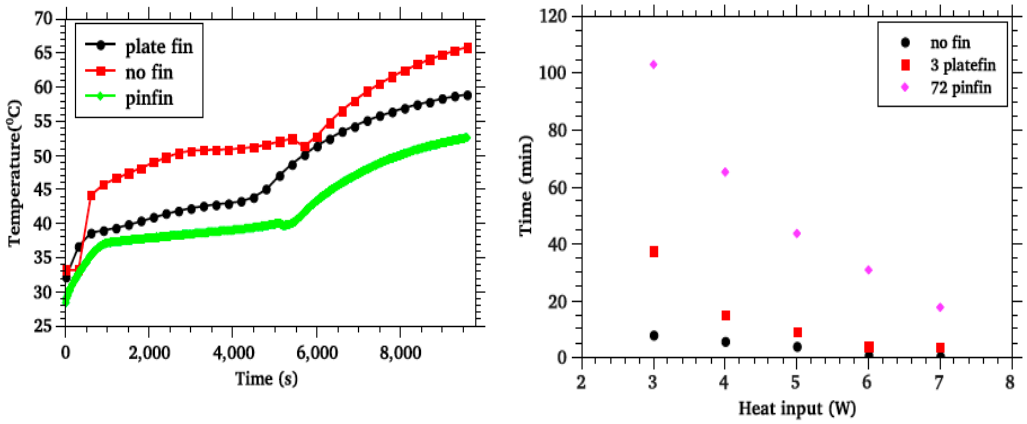

Figure 41. Comparison of heat sink base temperatures at 4W (left), comparison of time required for completion of phase change at separate power inputs (right). Source: [2].

From this data it can be concluded that PCM induced heat sinks with greater distribution across a conductive surface are much more effective at absorbing waste heat. That study concluded that because PCM itself has a low thermal conductivity, by using thermal conductivity enhancers such as pin fins to effectively distribute heat, the efficiency of the PCM is increased. With respect to the time taken to complete the phase change, an enhancement factor of 18 was observed for the PCM induced heat sink with pin fins vs. the heat sink with PCM and no thermal conductivity enhancers [2]. The contacted surface area/ distribution of the PCM with the thermal conductor is what greatly increases the efficiency of the PCM. It was calculated that the study done by Baby et al. [2] used approximately 59.5 g of n-eicosane for each heat sink compartment tested. By that measure, they achieved 0.2993 ºC of cooling affect for every gram of n-eicosane. Additionally, by the measure of PCM used, 1.69 minutes of cooling was achieved for every gram of n-eicosane used.

The analysis presented above, expressed in degrees Celsius per gram of PCM used, is the standard by which this thesis will be compared. Given that a greater distribution of PCM across the thermal conductor has been proven to improve the PCM efficiency, it could be assumed that introducing a PCM in the surface structure of aluminum, as conducted in this thesis, has the potential to increase PCM efficacy.

a. PCM Bath Heat Exchanger [2] vs. PCM Incorporated in the Surface of Aluminum and Coated with Epofix Epoxy

(1) FLIR Thermal Test

Comparing these results with the study conducted by Baby et al., 45.4 ºC of cooling was experienced for each gram of n-eicosane wax used, and the time to complete the phase change was 97.6 minutes for each gram of PCM used. By the first metric, the PCM induced anodic layer is 152 times more effective at cooling and 58 times more effective at holding a constant temperature throughout T_m. Even though this was initially promising, the Epofix epoxy was not repeatable due to leakage, and therefore no further analysis was performed.

b. PCM Bath Heat Exchanger [2] vs. PCM Incorporated in the Surface of Aluminum Coated with Silver Paint

(1) FLIR Thermal Test

In this thesis, 67 ºC of cooling was experienced for each gram of n-eicosane wax used, and the time to complete the phase change was 142 minutes for each gram of PCM used. By the first metric, the PCM induced anodic layer is 223 times more effective at cooling and 84 times more effective at holding a constant temperature throughout T_m than the literature study [2]. It is believed that because silver paint is more thermally conductive than the epoxy layer, this could greatly increase the conductor-PCM surface contact ratio, distributing the heat produced by the hot plate throughout the PCM itself.

(2) Thermocouple Test

In this thesis, when looking at the effects of incorporating PCM within the anodic structure vs. an anodic structure with no PCM, 24 ºC of cooling was experienced for each gram of n-eicosane wax used, and the time to complete the phase change was 172 minutes for each gram of PCM. By the first metric, the PCM layer is still 80 times more effective at lowering the rate of heating and 102 times more effective at holding constant throughout T_m than the study conducted by Baby et al. [2].

F. ROADMAP FOR IMPROVEMENTS

1. Improvements upon the Anodic Layer

After conducting this work, the need to explore other anodization conditions was identified. In this thesis, 25 minutes produced an AAO thickness of 10μm. Other studies have consistently created thicker anodic layers with larger pores, which have the potential to host more PCM.

By lowering the voltage/ current density, the pore growth rate is significantly decreased while the thickness of the anodic layer will continue to increase with time. In a study conducted by Moon et al. [32], oxalic acid was used to create a thick anodic layer with smaller pores. Chromic and phosphoric acid were used to increase the diameter of these pores through chemical etching. This resulted in a highly organized anodic layer at a

specific diameter. This was consistent enough to create membranes for collection and filtration of specific viruses. The AAO membrane had pore sizes of 75 +/- 5 nm in diameter of consistent thickness and aligned in the same orientation. These structures are shown in Figure 42. Aluminum foil was anodized in a 0.3 M oxalic acid bath at 5 ºC at a fixed voltage of 40 V for 20 hours. This anodic layer was removed with a 6 wt% phosphoric acid and 1.8 wt% chromic acid solution at 60 ºC. A second AAO layer was created by anodizing for 8 hours using the same conditions as the first stage of anodization and was followed by dissolution of the remaining aluminum in a HgCl2 solution. Pore widening was done through chemical etching in 0.8 wt% phosphoric acid held at 30 ºC for 60 minutes. This is the process that resulted in the highly ordered AAO pores with a cross sectional thickness of 24 μm [32].

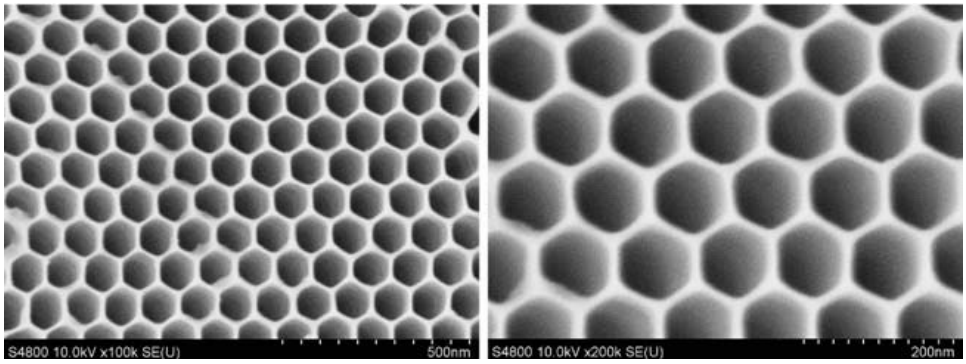

Figure 42. Field emisson scanning electron microscope (FE-SEM) images of the AAO membrane and further shrunk by atomic layer deposition. Source: [32].

While these anodic structures described in Figure 42 are extremely organized and have a desirable orientation and volume for PCM induction, we did not employed that method. One of the advantages of the technique we used is that it requires less time to generate the AAO layer.

2. Characterize the PCM AAO Layer Penetration

In this thesis, the PCM penetration into the AAO layer was not characterized because it requires a Cryo-SEM, but it's suggested for future steps. The study conducted

by Wu at al [31] was able to characterize the oil penetration into the anodic layer using Cryo-SEM. A sample of their images is show in in Figure 43. By characterizing the depth at which PCM is introduced in the AAO membrane, the concept of introducing PCMS in the surface layer could be further improved by ensuring that a maximum amount of PCM is embedded within the microstructure of the surface.

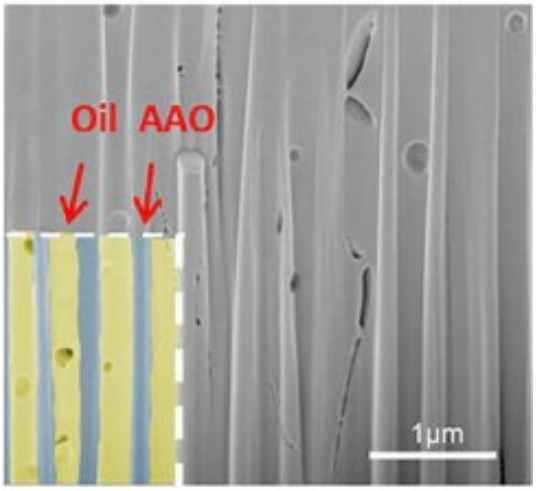

Figure 43. Cryo-SEM images of oil infused in AAO microchannels. Source: [31].

3. Improve the Conductivity of Sealants

Investigation of sealants that are more thermally conductive would contribute to the effectiveness of the PCM's latent heat energy storage potential. One study conducted by Fu et al. [33] applied alumina particles combined with boron nitride nano barbs to improve the thermal conductivity of epoxy adhesives. They found that by doing this the thermal conductivity was higher, electrical insulation was greater, and it provided improved mechanical strength. Another study conducted by Kim et al. [34] looked at epoxy molding compounds similar to what was used in this thesis. By filling epoxy molding compound with aluminum nitride particles at 70 percent by volume thermal conductivity improved by 5–8 times. Improving the thermal conductivity of the epoxy sealant would increase the contact ratio of thermal conductor to PCM.

IV. CONCLUSIONS AND RECOMMENDATIONS

A. CONCLUSIONS

The goal of this study was to engineer a surface layer that incorporates PCM into a metallic part at the microstructural level through a simple postproduction process that can be applied to existing, geometrically complex components.

An anodic layer was successfully fabricated on a given aluminum surface from an existing part. By adjusting the variables of electrolyte concentration, electrolyte temperature, time, and current density an anodic layer that contained pores with a diameter of 50 +/- 5 nm were able to be consistently created for use with various PCMs and sealant methods. Additionally, the effects of anodic layer overgrowth were characterized and compared with previous studies that formed AAO layers with oxalic acid.

The anodic layer was then annealed, a step that increased strength to the layer. Vacuum impregnation was employed to incorporate PCM into the porous AAO structure and sealed with various sealants. The vacuum impregnation chamber constructed as part of this work was highly effective at creating a vacuum seal. Additionally, this apparatus withstood multiple heating cycles during the vacuum impregnation process which was critical to the fabrication of multiple PCM incorporated AAO samples.

Through thermal testing, it was identified that the sealants that could withstand multiple cyclic loads were the silver and the HR epoxy. The silver coated sample displayed significant cooling with respect to the mass of n-eicosane used, while the HR epoxy was too insulative. Additionally, these thermal effects were measured multiple times with various methods of measurement (FLIR and thermocouples). When measured with k-type thermocouples, the PCM induced anodic layer coated with silver paint was 80 times more effective at lowering the rate of heating and 102 times more effective at holding constant throughout T_m than previously conducted studies where n-eicosane parrafin was applied to heat sinks for the application of cooling electronics.

A sample that showed promise in regard to significant heating rate reduction within T_m was the Epofix epoxy coated sample. However, this sample did not display the ability

to hold n-eicosane wax in liquid form under the experimental conditions employed, but with an improvement in epoxies and fabrication techniques these promising results could be replicated in a sample that could withstand cyclic thermal loads.

From the observed results compared with that of previous studies it can be said that greater distribution of PCM with a conductor's surface area allows the PCM to efficiently absorb any heat from the conductor. In this study, 0.05 grams of n-eicosane was not only spread throughout a small region but was partially impregnated within the anodic layer which greatly improves the surface area contact of the PCM-conductor. As a proof of concept, this study proved that the efficient application of the PCM within the microstructure can significantly decrease the peak transient thermal loads of the system into which the PCM is integrated.

With these effective results, latent heat energy storage could be achieved in more compact passive heat management devices, which would greatly reduce the size of electronic devices or push the boundaries of computing technology by reducing the thermal barrier impeding advancement. PCMs incorporated within the surface microstructure of components could be applied not only to electronic devices, but to machinery, and other systems employed by the DOD.

B. RECOMMENDATIONS

Improve the anodic layer. By creating a more consistent and organized AAO layer, the thermal properties of the latent heat energy storage system would be much more isotropic throughout the surface of the metallic substrate.

Scale up this method of PCM integration to geometrically complex parts. If all these advances could be made, this method of PCM usage can be significantly scaled up to a complex finned heat sink. There is great potential for application and scalability of PCM induction in AAO layers. By harnessing the full power of PCM latent heat energy storage, technology that was once restricted due to thermal management limits can be greatly improved upon.

LIST OF REFERENCES

[1] R. L. Helmick, B. G. Unkel, R. A. Cromis, and A. L. Hershey, "Development of an advanced air conditioning plant for DDG-51 class ships," *Nav. Eng. J.*, vol. 99, no. 3, pp. 112–123, May 1987, doi: 10.1111/j.1559-3584.1987.tb02123.x.

[2] R. Baby and C. Balaji, "Experimental investigations on phase change material based finned heat sinks for electronic equipment cooling," *Int. J. Heat Mass Transf.*, vol. 55, no. 5–6, pp. 1642–1649, Feb. 2012, doi: 10.1016/j.ijheatmasstransfer.2011.11.020.

[3] F. Wang, J. Cao, Z. Ling, Z. Zhang, and X. Fang, "Experimental and simulative investigations on a phase change material nano-emulsion-based liquid cooling thermal management system for a lithium-ion battery pack," *Energy*, vol. 207, p. 118215, Sep. 2020, doi: 10.1016/j.energy.2020.118215.

[4] R. Sabbah, R. Kizilel, J. R. Selman, and S. Al-Hallaj, "Active (air-cooled) vs. passive (phase change material) thermal management of high power lithium-ion packs: Limitation of temperature rise and uniformity of temperature distribution," *J. Power Sources*, vol. 182, no. 2, pp. 630–638, Aug. 2008, doi: 10.1016/j.jpowsour.2008.03.082.

[5] C. Veerakumar and A. Sreekumar, "Phase change material based cold thermal energy storage: Materials, techniques and applications – A review," *Int. J. Refrig.*, vol. 67, pp. 271–289, Jul. 2016, doi: 10.1016/j.ijrefrig.2015.12.005.

[6] E. Rodriguez-Ubinas, L. Ruiz-Valero, S. Vega, and J. Neila, "Applications of Phase Change Material in highly energy-efficient houses," *Energy Build.*, vol. 50, pp. 49–62, Jul. 2012, doi: 10.1016/j.enbuild.2012.03.018.

[7] R. Kumar, S. Vyas, R. Kumar, and A. Dixit, "Development of sodium acetate trihydrate-ethylene glycol composite phase change materials with enhanced thermophysical properties for thermal comfort and therapeutic applications," *Sci. Rep.*, vol. 7, no. 1, p. 5203, Dec. 2017, doi: 10.1038/s41598-017-05310-3.

[8] Hongyu Zhang, Chunlong Zhuang, Limin Li, A. Deng, Shengbo Li, and Xiaodong Shen, "Analyse on the characteristic of cooling load in light weight PCM building," in *2011 Second International Conference on Mechanic Automation and Control Engineering*, Inner Mongolia, China, Jul. 2011, pp. 2869–2872. doi: 10.1109/MACE.2011.5987586.

[9] C. S. Malvi, D. W. Dixon-Hardy, and R. Crook, "Energy balance model of combined photovoltaic solar-thermal system incorporating phase change material," *Sol. Energy*, vol. 85, no. 7, pp. 1440–1446, Jul. 2011, doi: 10.1016/j.solener.2011.03.027.

[10] K. A. R. Ismail and J. R. Henríquez, “Thermally effective windows with moving phase change material curtains,” *Appl. Therm. Eng.*, vol. 21, no. 18, pp. 1909–1923, Dec. 2001, doi: 10.1016/S1359-4311(01)00058-8.

[11] X. Huang, G. Alva, Y. Jia, and G. Fang, “Morphological characterization and applications of phase change materials in thermal energy storage: A review,” *Renew. Sustain. Energy Rev.*, vol. 72, pp. 128–145, May 2017, doi: 10.1016/j.rser.2017.01.048.

[12] A. Sharma, V. V. Tyagi, C. R. Chen, and D. Buddhi, “Review on thermal energy storage with phase change materials and applications,” *Renew. Sustain. Energy Rev.*, vol. 13, no. 2, pp. 318–345, Feb. 2009, doi: 10.1016/j.rser.2007.10.005.

[13] K. Faraj, M. Khaled, J. Faraj, F. Hachem, and C. Castelain, “Phase change material thermal energy storage systems for cooling applications in buildings: A review,” *Renew. Sustain. Energy Rev.*, vol. 119, p. 109579, Mar. 2020, doi: 10.1016/j.rser.2019.109579.

[14] T. Silva, R. Vicente, C. Amaral, and A. Figueiredo, “Thermal performance of a window shutter containing PCM: Numerical validation and experimental analysis,” *Appl. Energy*, vol. 179, pp. 64–84, Oct. 2016, doi: 10.1016/j.apenergy.2016.06.126.

[15] E. Arce, R. Agrawal, A. Suárez, L. Febrero, and C. C. Luhrs, “Modeling of Energy Demand and Savings Associated with the Use of Epoxy-Phase Change Material Formulations,” *Materials*, vol. 13, no. 3, p. 639, Jan. 2020, doi: 10.3390/ma13030639.

[16] M. H. M. Isa, X. Zhao, and H. Yoshino, “Preliminary Study of Passive Cooling Strategy Using a Combination of PCM and Copper Foam to Increase Thermal Heat Storage in Building Facade,” *Sustainability*, vol. 2, no. 8, pp. 2365–2381, Jul. 2010, doi: 10.3390/su2082365.

[17] A. Siricharoenpanich, S. Wiriyasart, A. Srichat, and P. Naphon, “Thermal management system of CPU cooling with a novel short heat pipe cooling system,” *Case Stud. Therm. Eng.*, vol. 15, p. 100545, Nov. 2019, doi: 10.1016/j.csite.2019.100545.

[18] C.-T. Chen, C.-K. Wu, and C. Hwang, “Optimal Design and Control of CPU Heat Sink Processes,” *IEEE Trans. Compon. Packag. Technol.*, vol. 31, no. 1, pp. 184–195, Mar. 2008, doi: 10.1109/TCAPT.2008.916855.

[19] C. H. Jeong, H. R. Kim, M. Y. Ha, S. W. Son, J. S. Lee, and P. Y. Kim, “Numerical investigation of thermal enhancement of plate fin type heat exchanger with creases and holes in construction machinery,” *Appl. Therm. Eng.*, vol. 62, no. 2, pp. 529–544, Jan. 2014, doi: 10.1016/j.applthermaleng.2013.09.044.

[20] M. K. Choi, “Using Paraffin PCM to Make Optical Communication Type of Payloads Thermally Self-Sufficient for Operation in Orion Crew Module,” presented at the 14th International Energy Conversion Engineering Conference, Salt Lake City, UT, Jul. 2016. doi: 10.2514/6.2016-4601.

[21] Loura Hall, “NASA to Begin Testing Next Generation of Spacecraft Heat Exchangers.,” NASA, Aug. 2017. Accessed: May 08, 2022. [Online]. Available: https://www.nasa.gov/feature/nasa-to-begin-testing-next-generation-of-spacecraft-heat-exchangers

[22] C. J. Ho, P.-C. Chang, W.-M. Yan, and M. Amani, “Microencapsulated n-eicosane PCM suspensions: Thermophysical properties measurement and modeling,” *Int. J. Heat Mass Transf.*, vol. 125, pp. 792–800, Oct. 2018, doi: 10.1016/j.ijheatmasstransfer.2018.04.147.

[23] K. P. Bloschock and A. Bar-Cohen, “Advanced thermal management technologies for defense electronics,” Baltimore, Maryland, USA, May 2012, p. 84050I. doi: 10.1117/12.924349.

[24] M. Paz Martínez-Viademonte, S. T. Abrahami, T. Hack, M. Burchardt, and H. Terryn, “A Review on Anodizing of Aerospace Aluminum Alloys for Corrosion Protection,” *Coatings*, vol. 10, no. 11, p. 1106, Nov. 2020, doi: 10.3390/coatings10111106.

[25] O. Sanz, F. J. Echave, J. A. Odriozola, and M. Montes, “Aluminum Anodization in Oxalic Acid: Controlling the Texture of Al_2O_3/Al Monoliths for Catalytic Aplications,” *Ind. Eng. Chem. Res.*, vol. 50, no. 4, pp. 2117–2125, Feb. 2011, doi: 10.1021/ie102122x.

[26] J. Zhang *et al.*, “Anodization of aluminum in a sealed container,” *Electrochem. Commun.*, vol. 129, p. 107086, Aug. 2021, doi: 10.1016/j.elecom.2021.107086.

[27] A. Christoulaki, S. Dellis, N. Spiliopoulos, D. L. Anastassopoulos, and A. A. Vradis, “Controlling the thickness of electrochemically produced porous alumina membranes: the role of the current density during the anodization,” *J. Appl. Electrochem.*, vol. 44, no. 6, pp. 701–707, Jun. 2014, doi: 10.1007/s10800-014-0680-4.

[28] Huong Le and J. Watcher, “Comparison of sulfuric and oxalic acid anodizing for preparation of thermal control coatings for spacecraft,” presented at the Support the Highway to Space Through Testing, Goddard Space Center, Jan. 1988. Accessed: May 08, 2022. [Online]. Available: https://ntrs.nasa.gov/api/citations/19890003246/downloads/19890003246.pdf

[29] I. V. Roslyakov *et al.*, “Annealing induced structural and phase transitions in anodic aluminum oxide prepared in oxalic acid electrolyte,” *Surf. Coat. Technol.*, vol. 381, p. 125159, Jan. 2020, doi: 10.1016/j.surfcoat.2019.125159.

[30] M. Montazer and T. Harifi, “Nanoencapsulation techniques for textile finishing,” in *Nanofinishing of Textile Materials*, Elsevier, 2018, pp. 295–310. doi: 10.1016/B978-0-08-101214-7.00019-4.

[31] D. Wu *et al.*, “Durable lubricant-infused anodic aluminum oxide surfaces with high-aspect-ratio nanochannels,” *Chem. Eng. J.*, vol. 368, pp. 138–147, Jul. 2019, doi: 10.1016/j.cej.2019.02.163.

[32] J.-M. Moon, D. Akin, Y. Xuan, P. D. Ye, P. Guo, and R. Bashir, “Capture and alignment of phi29 viral particles in sub-40 nanometer porous alumina membranes,” *Biomed. Microdevices*, vol. 11, no. 1, pp. 135–142, Feb. 2009, doi: 10.1007/s10544-008-9217-0.

[33] J. Fu, L. Shi, D. Zhang, Q. Zhong, and Y. Chen, “Effect of nanoparticles on the performance of thermally conductive epoxy adhesives,” *Polym. Eng. Sci.*, vol. 50, no. 9, pp. 1809–1819, Sep. 2010, doi: 10.1002/pen.21705.

[34] W. Kim, J.-W. Bae, I.-D. Choi, and Y.-S. Kim, “Thermally conductive EMC (epoxy molding compound) for microelectronic encapsulation,” *Polym. Eng. Sci.*, vol. 39, no. 4, pp. 756–766, Apr. 1999, doi: 10.1002/pen.11464.

INITIAL DISTRIBUTION LIST

1. Defense Technical Information Center
   Ft. Belvoir, Virginia

2. Dudley Knox Library
   Naval Postgraduate School
   Monterey, California